8-2018

Modeling Dynamics of Gel-Based Composites Under Ferromagnetic Resonance Heating

Oksana Savchak
Clemson University, osavcha@g.clemson.edu

MODELING DYNAMICS OF GEL-BASED COMPOSITES UNDER FERROMAGNETIC RESONANCE HEATING

A Thesis
Presented to
the Graduate School of
Clemson University

In Partial Fulfillment
of the Requirements for the Degree
Master of Science
Materials Science and Engineering

---

by
Oksana Savchak
August 2018

Accepted by:
Dr. Olga Kuksenok, Committee Chair
Dr. Konstantin G. Kornev
Dr. Igor Luzinov

ABSTRACT

Designing soft, active materials that change their shape and properties depending on external stimuli is a rapidly developing area of research. Using theoretical and computational modeling, we focus on the dynamics of gel filled with uniformly distributed ferromagnetic nanoparticles exposed to electromagnetic (EM) waves in the GHz frequency range. For the polymer matrix, we choose Poly(N-isopropylacrylamide) (PNIPAAm) gels, which have a lower critical solution temperature and shrinks upon heating. When these composites are irradiated with EM waves that have frequency close to that of the Ferro-Magnetic Resonance (FMR) frequency, the heating rate increases dramatically. The magnetically induced heating inside the nanoparticles is transferred to the gel matrix. We show that the dissipated EM energy causes volume phase transitions in the gel, as a response to temperature change, leading to the large deformations of the sample for a range of system parameters. We propose a model that accounts for the dynamic coupling between the elastodynamics of polymer gels and FMR heating of magnetic nanoparticles. This coupling is non-linear: as the system is heated and the gel shrinks at the temperatures close to the volume phase transition temperature, the particles concentration increases, which in turn results in an increase of the heating rates as long as the concentration of nanoparticles does not exceed a critical value. We show that the system exhibits high selectivity to the frequency of the incident EM radiation and can result in a large mechanical feedback in response to the time-varying power signal. These results suggest a design of a new class of soft active gel-based materials remotely controlled by the low power EM signals within the GHz frequency range.

ACKNOWLEDGMENTS

First of all, I would like to thank my advisor, Dr. Olga Kuksenok, for giving me the opportunity to work in her group. I am very grateful for the words of encouragement (especially at difficult moments), her patient, caring attitude, and her professional guidance through my study. I really respect her for her positive attitude to life and to work. I cannot go on without thanking my husband, Mykhailo Savchak, because he is the one who encouraged me to study; without his belief and support I would never have taken the initiative to follow my dreams.

Thank you to Dr. Konstantin Kornev and Dr. Igor Luzinov for their willingness to be part of my committee and for their useful comments to my research. I really appreciate Dr. Kornev's patience and readiness to help. It was his actions and his behavior that helped me to believe in my capabilities to study and build the confidence to conquer the unknown. I am especially grateful to Dr. Luzinov for his assistance with the questions regarding the study process. I truly admire his openness and honesty to be able to say "I don't know this", because it helped me to feel better about the material I didn't fully understand.

I would like to acknowledge Tyler Morrison, who along with Dr. Olga Kuksenok introduced me to gLSM, and for writing a magnetic modulus for M-gLSM. Also, thank you to Chinmay Sonar for the collaboration and for some data analysis.

I would like to express my gratitude to Dr.Yu Gu for answering my questions regarding his work on magnetic heating throughout these two years.

A special thanks to Dr. Ulf Schiller for coming to our office at the right time, especially when I was in need for some explanations. I appreciate his personality as an approachable teacher.

I owe a big thank to my teacher of Electromagnetism, Dr. Lu Xian. Because of her great teaching skills, I have fallen in love with this subject, which has helped me to better understand my research. I also recognize Dr. Jian He for his willingness to help me in understanding some material and his amazing teaching talent.

I would like to extend my appreciation to my dear friend and English teacher, Sandra Kluck, for her great job in helping me to improve my English grammar. I am so grateful that God placed her in my life.

I would also like to acknowledge my colleagues and group members Yao Xiong, Sidong Tu, Chandan Choudhury, Vaibhav Palkar, Mehrdad Yousefi, and Fang Wang for their support and encouragement during my stay at Clemson University. I will always remember these happy moments when we ate cakes, drank tea, and laughed. Additional thanks to Dr. Olga Kuksenok and Dr. Ulf Schiller for organizing these happy moments for us.

Also I would like to thank my family and friends for the support and encouragement during this study program.

TABLE OF CONTENTS

Page

LIST OF FIGURES

CHAPTER 1

INTRODUCTION

The gel-based stimuli-responsive composite materials have been actively studied in recent years. Because of their unique properties to change volume or chemical composition in response to external stimuli, such as pH, temperature, solvent composition, magnetic field, etc. [1], they are often called "smart" materials. The applications of these stimuli-responsive hydrogels are often limited because of their finite response properties. Recently, much work has been done to resolve this issue through the integration of nanomaterials (ceramic or metal nanoparticles, carbon nanotubes, etc.) into hydrogel matrix [2]. For example, adding gold nanoparticles to hydrogels enhances their electrical conductivity [2], while impregnation of graphene and graphene oxide in natural hydrogels is used to reinforce the strength of hydrogel composites [2]. The incorporation of magnetic nanoparticles into host polymer networks can offer straightforward methods to enhance the responsiveness of hydrogel composites to an electromagnetic (EM) signals [3-6]. These magnetically responsive composite hydrogels, which offer the advantage of remote control [7], could be used for development of a range of remotely controlled soft coatings, sensors, and actuators. Controlling dynamics of these materials by the low power electromagnetic (EM) wave within the GHz frequency range is of particular interest given an extensive usage of GHz bands in various communication protocols. For example, Bluetooth technologies operate at 2.4 GHz and 5GHz frequencies, while Metropolitan Area Network (MAN) protocols and radars operate within a wide range of GHz bands [8]. Developing soft active reconfigurable materials that would ultimately allow one to control mechanical

actuation, shape, or wetting properties through the usage of the existing communication protocols could be beneficial for a range of applications.

In our research we focus on the design of soft gel-based magnetic composites that are magneto- and thermo-responsive. The goal is to identify conditions leading to large elastic deformations upon electromagnetic heating of these composites within the GHz frequencies range. The most important characteristics of these systems is that the magnetic heating is non-linearly coupled with the gel's dynamics, resulting in a large-scale deformation of the temperature-responsive gel composite when interacting with an EM field.

In this work we consider only stable chemically cross-linked hydrogels. Since Poly(N-isopropylacrylamide) (PNIPAAm) is a well-studied thermoresponsive hydrogel, we chose it as a polymer matrix. These hydrogels shrink upon heating at above their Volume Phase Transition Temperature (VPTT) [9]. We examined low concentrations of single-domain magnetic nanoparticles (NPs) (initial NPs concentration does not exceed 1% in the simulations below) that are assumed to be uniformly distributed inside the gel matrix. The nanoparticles (NPs) could either be covalently grafted into the polymer network or physically trapped within it [10]. To prevent the aggregation of the nanoparticles within the gel during the sample preparation, NPs could be coated to ensure compatibility with the gel matrix [11]. These nanoparticles effectively act as heat generators when they are exposed to an alternating current (AC) field. [12]. In our research we studied the heating efficiency for the two types of nanoparticles (cobalt and magnetite), with more focus on cobalt nanoparticles.

A number of prior studies demonstrated an efficiency of heating of hydrogels filled with superparamagnetic nanoparticles [13-17]. In these studies, a typical frequency of the AC EM signal is on the order of hundreds of kHz and the heating is due to the combination of Neel (flipping of spins) and Brownian (viscous friction between rotating NPs and matrix) relaxation [18, 19]. The possible applications of these hydrogels filled with magnetic nanoparticles range from biomedical drug delivery (often for hyperthermia treatments) [20, 21] to utilizing external EM signals for the remote control of hydrogel membrane porosity for the well-targeted molecular sieving [22]. Either PNIPAAm gels [5, 23] or various copolymers, including PNIPAAm gels [24, 25], are used in the studies of nanoparticle-hydrogel composites.

In our work we focused on the GHz band frequencies, where the mechanism of the gel heating is distinctly different [26, 27]. The previously estimated heating rates of non-deformable composites, such as paraffin films filled with various magnetic nanoparticles at GHz frequencies [27], support the feasibility of using these frequencies to control the temperature of the system and, as a result, the volume phase transitions in thermo-responsive hydrogels. With regard to the hydrogels filled with ferromagnetic nanoparticles investigated here, we separate the effects of magnetic heating caused by the interaction of the EM wave with ferromagnetic NPs from the dielectric heating of the hydrogel matrix (neglecting the last one). While water is well known to absorb microwaves (GHz frequencies band) [28] and would result in dielectric losses within the gel matrix, magnetic nanoparticles are shown to significantly enhance the localized selective microwave heating [29, 30] and providing a significantly greater contribution from the magnetic heating than

from the corresponding dielectric heating [29]. To account for the effect of external mechanical deformations, these films could be placed on a metal substrate in the respective experiments; for thin films with the thicknesses much smaller than the wavelength of the EM wave, the electric component of the EM wave will be reflected from the metal [31].

We have developed a model that couples heating of magnetic nanoparticles within the GHz frequency range [27] with the gel elastodynamics in three dimensions [32]. We then focus on mechanical response of these gel-nanoparticle composites to the applied EM waves. In the simulations below, we assume that the sample is thermally insolated. Finally, the thermal diffusion coefficient is a few orders of magnitudes greater than the collective diffusion coefficient of the polymer network [33]. Consequently, we assume that the temperature is uniform within the gel samples at any given moment in time for the sample sizes considered in this work.

CHAPTER 2

THEORETICAL BACKGROUND

2.1: Magnetism in Nanoparticles

In chapter two we discuss the essence of magnetism and explain the derivation of formulas of the heating rate and introduce the description of properties of polymer gels based on literature. These concepts will be the basis of the computational experiments in this thesis.

Nanomagnetism is an active and highly interesting topic in science. It has had an impact in all areas of life, from geology to magnetic recording to biomedical applications [34]. The nanoscience is dealing with the objects that are in the range from 1nm to 100 nm (same range as the sizes of many viruses and macromolecules) [34], thus magnetic nanoparticles are widely applied in nanomedicine, particularly in the field of cancer treatment. In our work we focus on how to exploit the benefits of heat induction by magnetic nanoparticles (exposed to EM signal) for the development of new composite materials. Therefore it is important to understand the fundamentals of magnetism in nanoparticles and the main parameters controlling the heating process in the composite. By choosing the right type of magnetic material one can achieve the desired heating effect.

Materials possess different degrees of magnetism that can be classified as diamagnetic, paramagnetic, and ordered magnetic materials (ferrimagnetic, antiferromagnetic, and ferromagnetic). The vast majority of the materials are diamagnetic and have very weak magnetization that is opposite of the applied magnetic field [35].

Paramagnetic materials have a higher degree of magnetization due to the presence of unpaired electrons. However, paramagnetic materials are magnetically disordered. Ferromagnetic materials (iron, nickel, and cobalt) have the most striking magnetic properties at room temperature [36]. Nevertheless, even they lose their magnetic properties at high temperatures, which is specific for each material.

Magnetic properties of materials can be understood from classical and quantum mechanical points of view. The classical model is simpler, and based on it, magnetism arises due to the electron motion around its orbit (around a nucleus) and around its own axis (like the earth rotates around its axis). Matter is made out of atoms, which contain electrons revolving around a nucleus. The rotation of charged particles gives rise to an effective magnetic moment [37]. The orbital and spin motion of an unpaired electron comprises a total magnetic moment of a single atom. In solid material, magnetic moments of atoms can be grouped together and aligned, creating regions which are called magnetic domains. Each domain is a net magnetization of a particular region with a direction that is different from its neighbor. Magnetization (magnetic polarization) is a density of magnetic dipole moments that is induced in a magnetic material when it is exposed to an external magnetic field [37]. Classical physics gives a basic explanation of the mechanics of magnetism. However, as knowledge of this concept has increased and gone further into the mathematical description of magnetism, quantum mechanics has given more accurate explanations [36]. Nevertheless, we will use classical electromagnetic formulation.

The dimensions of nanoparticles strongly influence their magnetic behavior. Smaller nanoparticles can be considered as single-domain, and larger nanoparticles, above some critical diameter - as a multidomain [34]. Small ferromagnetic or ferrimagnetic nanoparticles, which are single domain, exhibit a phenomenon known as a superparamagnetism. The critical diameters vary for different types of nanoparticles. For instance, the approximate diameter of cobalt nanoparticles, which appear to have superparamagnetic behavior under the standard conditions, is below 10 nm, while for magnetite (Fe_3O_4) is below 30 nm [18]. However, above these values, nanoparticles would be just a single domain nanoparticles. When the particle size decreases, the domain walls in ferromagnetic NPs disappear, approaching critical radius, r_c , and with further decrease a particle enters a superparamagnetic regime. To illustrate these transition points between superparamagnetic, single-domain, and multi-domain regions, Figure 2.1 was adapted from the reference [35].

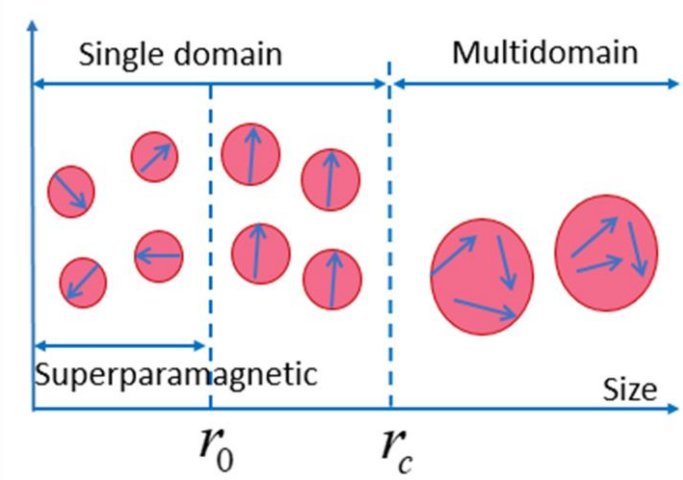

Figure 2.1 Transition of the magnetic regimes (superparamagnetic, single-domain, multi-domain) as a function of nanoparticles size.

It is worth noting that all superparamagnetic nanoparticles are single-domain particles, but not always single-domain particles are superparamagnetic [38].

Magnetic nanoparticles (MNPs) can be in the form of pure material like Co, Fe, Ni or they can be made out in the form of alloys. Their application will be defined based on their properties. For example, platinum-based MNPs show great stability in water [39] and are used as a contrast agent for MRI and X-ray computed tomography [40]. The most commonly used nanoparticles for biomedical application are iron oxide, in particular magnetite (Fe_3O_4) and maghemite ($\gamma - Fe_2O_3$) due to their chemical stability, biocompatibility, and relatively low fabrication cost [39]. Cobalt NPs have high values of saturation magnetization that could result in a high thermal energy dissipation.

In order to analyze and predict the behavior of magnetic materials one must know their basic parameters: anisotropy constant and saturation magnetization. Magnetic anisotropy shows the change in internal energy of a material when the direction of magnetization is changed [41]. In our calculations we took into account two of the most common types of anisotropy: magnetocrystalline and shape anisotropies.

Magnetocrystaline anisotropy results from spin-orbit coupling, which is combined with the crystal lattice. It is related to the alignment of magnetization vectors along a specific, energetically favored crystallographic direction known as easy axes. The magnetocrystaline anisotropy is usually much greater in nanoparticles than that in analogous bulk solids [42].

If one wants to magnetize a spherical sample, the magnetization will be distributed to the same extent in all directions. However, an ellipsoidal sample is easier to magnetize along the long axis than along a short one [43]. It can be explained based on the demagnetization field, which is stronger along the short axis, meaning that a greater field needs to be applied in this direction to create a responsive field inside the specimen. Hence, the shape by itself can be a source of magnetic anisotropy. When a specimen (in our case nanoparticles) of defined shape is magnetized by an external magnetic field, the magnetic poles appear on its ends and tend to oppose the direction of the applied field [37]. This field is called a demagnetization field. The shape anisotropy of the sample can be described quantitatively by the demagnetization tensor N (derived from the demagnetization field), which depends on the shape.

When choosing the type of nanoparticles for a specific application (superparamagnetic or ferromagnetic single-domain nanoparticles) several parameters should be taken into account: heating efficiency, colloidal stability, and tendency to oxidation. The size, shape, and composition of nanoparticles can be modified to tailor the magnetic properties to a specific application [44].

2.2: Hydrogels: Definitions and Applications

Hydrogels are water-swollen polymeric cross-linked networks that maintain a distinct three-dimensional shape. The widely-used type of hydrogels are chemically cross-linked (e.g., PNIPAAm), which means that polymer chains are covalently bonded. Unlike chemically cross-linked hydrogels, physically cross-linked gels typically have weaker

connections that are held together by hydrogen bonds, electrostatic forces, or chain entanglements [45]. Hydrogels are also categorized based on their polymer origin, natural or synthetic. PNIPAAm is a synthetic polymer made from acrylamide monomers.

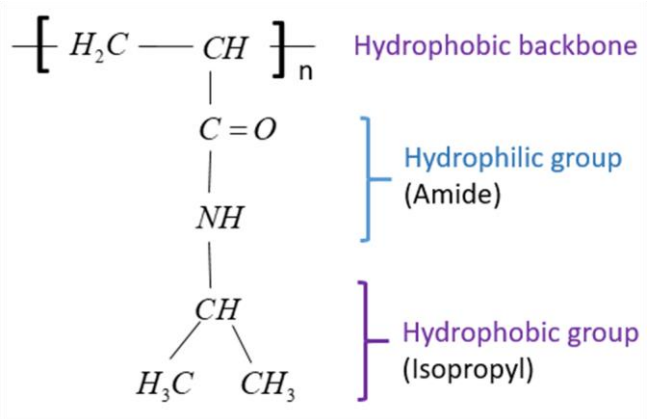

Figure 2.2 Chemical structure of poly (N-isopropylacrylamide) (PNIPAAm)

The thermoresponsive behavior of PNIPAAm originates from a delicate balance between the hydrophobic (isopropyl) and hydrophilic (amide) moieties that are interconnected with water molecules through hydrogen bonding. At high temperatures intermolecular hydrogen bonds break up (water molecules are expelled from the hydrogel matrix) and intramolecular interactions between amide and isopropyl groups become predominant; as a result, the polymer structure collapses [46]. Thus, PNIPAAm hydrogels undergo shrinking upon heating above the critical temperature, which is called Volume Phase Transition (VPT) temperature. For PNIPAAm hydrogel this temperature is around 32-33^{0}C [9].

As was mentioned in the introduction, combining these two materials (thermoresponsive hydrogels and magnetic nanoparticles), with the above described

unique properties, opens up an opportunity for developing novel synthetic nanocomposite materials.

CHAPTER 3

MODELING THE SYSTEM: M-gLSM

We first developed a model that captures magnetic heating of the gel composite within the GHz frequency range coupled with the gel's elastodynamics, which is modeled based on the gel Lattice Spring Model (gLSM) [32, 47, 48]. Originally, the gLSM [32, 47, 48] was developed to simulate the dynamics of self-oscillating gels undergoing the Belousov-Zhabotinsky chemical reactions[49]. The Gel Lattice Spring Model combines governing reaction-diffusion equations for reagents (between the gel and fluid) and gel dynamics equations. A number of computational studies using gLSM have shown the reliability of this model; the simulation results are in good agreement with the corresponding experimental results [32, 50-53]. Thereby, this approach is an effective tool for simulating the dynamics of a variety of chemo-responsive gels. In this work the three-dimensional gLSM framework was adapted to simulate the effects of interactions of the EM wave and a gel composite filled with magnetic nanoparticles; from this point we will refer to this framework as M-gLSM. The magnetic contribution of this model is based on the Ferromagnetic Resonance (FMR) theory, which involves the corresponding boundary value problem of electrodynamics [27]. The schematic of the FMR setup (Figure 3.1a) helps to visualize our computational experiments.

3.1 Governing Equations of the Gel Elastodynamics

Within the gLSM [32, 47, 48], the total energy of chemo-responsive gels is taken as a sum of energy of the polymer-solvent interaction, U_{FH}, and elastic energy associated with the gel deformation, U_{el}. The first term is written in the following Flory-Huggins form [54]:

$$U_{FH} = \sqrt{I_3}[(1-\varphi)\ln(1-\varphi) + \chi_{FH}(\varphi,T)\varphi(1-\varphi)] \tag{3.1}$$

Here, φ is the volume fraction of the polymer, 1-φ is the volume fraction of solvent, and $\chi_{FH}(\varphi,T)$ is the Flory-Huggins polymer-solvent interaction parameter. Finally, $I_3 = \det \hat{\mathbf{B}}$ in Equation (3.1) is an invariant of the left Cauchy-Green (Finger) strain tensor $\hat{\mathbf{B}}$, that is related to the volume changes of the deformed gel [55]. The elastic energy contribution to the total energy, U_{el}, describes the rubber elasticity of the cross-linked network [54, 56], and is proportional to the crosslink density, c_0:

$$U_{el} = \frac{c_0 \upsilon_0}{2}(I_1 - 3 - \ln I_3^{1/2}), \tag{3.2}$$

where υ_0 is the volume of a monomeric unit and $I_1 = tr\hat{\mathbf{B}}$ [55]. The constitutive equation for the chemo-responsive gels reads [47]:

$$\hat{\boldsymbol{\sigma}} = -P(\varphi,T)\hat{\mathbf{I}} + c_0\upsilon_0\frac{\varphi}{\varphi_0}\hat{\mathbf{B}}, \tag{3.3}$$

where $\hat{\boldsymbol{\sigma}}$ is the dimensionless stress tensor measured in units of $\upsilon_0^{-1}kT$, $\hat{\mathbf{I}}$ is the unit tensor, φ_0 is the volume fraction of the polymer at preparation, and $P(\varphi,T)$ is the isotropic pressure defined as [9, 47]

$$P(\varphi,T) = -(\varphi + \ln(1-\varphi) + \chi(\varphi,T)\varphi^2) + c_0\upsilon_0\varphi(2\varphi_0)^{-1}. \tag{3.4}$$

The parameter $\chi(\varphi,T)$ in the above equation is a function of both polymer volume fraction and temperature, *T*, and is found as [9]

$$\chi(\varphi,T) = \chi_0(T) + \chi_1(\varphi)\ , \tag{3.5}$$

where $$\chi_0(T) = [\delta h - T\delta s]/kT\ , \tag{3.6}$$

with δh and δs being the respective changes in the enthalpy and entropy per monomeric unit of the gel. In the elastomagnetic composite, an absorption of the EM wave results in the heating of the sample, which in turn leads to the dependence of $\chi_0(T)$ on the EM wave frequency and the respective changes in the equilibrium degree of swelling. This equilibrium degree of swelling as a function of T is found as [32]

$$\lambda_{eq}(T) = (\varphi_0 / \varphi_{eq}(T))^{1/3}, \tag{3.7}$$

where an equilibrium volume fraction of the polymer, $\varphi_{eq}(T)$, for an unconstrained three-dimensional sample is found by requiring $\hat{\boldsymbol{\sigma}}$ = 0 (eq. 3.3) in equilibrium [32]:

$$c_0\upsilon_0[(\frac{\varphi_{eq}}{\varphi_0})^{1/3} - \frac{\varphi_{eq}}{2\varphi_0}] = -(\varphi_{eq} + \ln(1-\varphi_{eq}) + [\chi_0(T) + \chi_1\varphi_{eq}]\varphi_{eq}{}^2) \tag{3.8}$$

The details of the three-dimensional formulation and implementation of the gLSM approach are provided in Reference [32].

3.2 Governing Equations for the Magnetic Heating

The schematic of ferromagnetic resonance (FMR) setup is shown in Figure 3.1a. A gel layer filled with magnetic NPs is placed in a DC magnetic field ($\mathbf{H}_{ex}$), and an EM wave is applied along the direction of $\mathbf{H}_{ex}$. It is important to emphasize that the magnetic component of the EM wave, $\mathbf{h}_{0,}$ is perpendicular to $\mathbf{H}_{ex}$ (in blue in Figure 4.1a). When the applied microwave frequency coincides with the natural precession frequency of a spin system, the amplitude of the precession becomes larger, and the maximum absorption is observed. This phenomenon is known as resonance. FMR is a useful technique to examine magnetic properties of ferromagnetic materials, such as magnetic anisotropies and the Gilbert-damping coefficient [57]. The experimental setup includes the following: an EM wave excitation source, an electromagnet, and a detector (as shown in Figure 4.1a).The detection of resonance could be done in two ways: 1) one could either vary the strength of the external field, keeping an applied frequency of the AC field fixed, or 2) to fix the external field and scan over a range of frequencies. In our simulations, we keep $\mathbf{H}_{ex}$ constant and vary the frequency of the AC field.

In the absence of the magnetic field, the magnetic dipole moments of each nanoparticle are randomly oriented in the polymer matrix. By adding the external magnetic field, the net magnetic dipole moments (magnetization vectors **M)** are aligned along the z-direction; the field inside the composite is disturbed and dissimilar to the $\mathbf{H}_{ex}$.

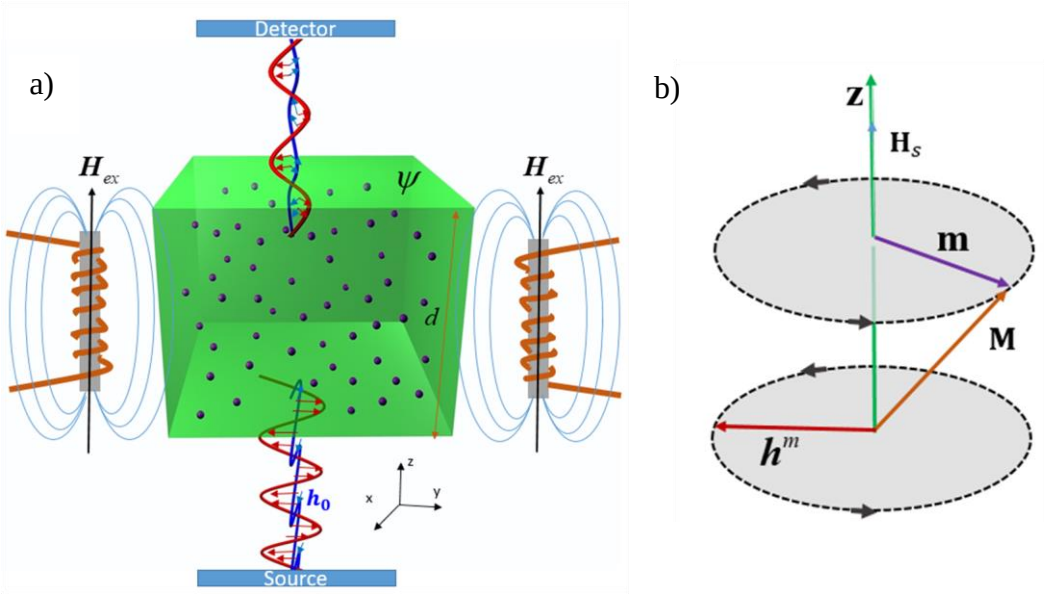

Figure 3.1: (a) Schematic of the gel composite under the FMR heating. A gel layer filled with magnetic nanoparticles is subjected to a bias DC magnetic field, $\mathbf{H}_{ex}$, and an EM wave with the magnetic field $\mathbf{h_0}$ perpendicular to $\mathbf{H}_{ex}$ is applied in z-direction. Nanoparticles are assumed to be uniformly distributed and trapped within the gel matrix; (b) Damped precession of a magnetic moment, **M**, toward the magnetic field $\mathbf{H}_s$ for a single domain nanoparticle; **m** is the xy-projection of the magnetization vector **M**.

Assuming that the easy axes of the nanoparticles are oriented parallel to the DC magnetic field, then the magnetic field within the gel film can be found as [27] :

$$\mathbf{H}_{in} = \mathbf{H}_{ex} - \psi \mathbf{M}, \tag{3.9}$$

where $\mathbf{M}$ is a magnetization for the single nanoparticle. Only when all magnetization vectors are aligned in the same direction can maximum absorption of the EM wave be achieved. In the absence of the EM wave, the bias direct current (DC) field inside the magnetic NP, $\mathbf{H}_s$, depends on [27]: i) internal field $\mathbf{H}_{in}$; ii) the effective field caused by the magnetocrystalline anisotropy $\mathbf{H}_a$; iii) the demagnetization field $\mathbf{H}_d$.

$$\mathbf{H}_s = \mathbf{H}_{in} + \mathbf{H}_a + \mathbf{H}_d \tag{3.10}$$

For the case of uniaxial magnetocrystalline anisotropy, introduced in Chapter 2, $\mathbf{H}_a = \left(2K_1 / \mu_0 M_s\right)\mathbf{z}$, where M_s is a saturation magnetization of the material, K_1 is a constant of magnetocrystalline anisotropy, μ_0 is a permeability of a vacuum, and $\mathbf{z}$ is a unit vector along the vertical direction in Figure 3.1a. The demagnetization field, which is shape dependent, is $\mathbf{H}_d = -M_s\mathbf{z}/3$, with the demagnetizing factor for the spherical nanoparticle being $N = 1/3$ [57].The applied AC field destabilizes the orientation of the magnetization vector, resulting in the precession of this vector around the z-axis (Figure 3.1b), which is described by the Landau-Lifshitz-Gilbert equation (LLG) [26, 31]:

$$\frac{d\mathbf{M}}{dt} = -\gamma\mu_0\left[\mathbf{M}\times(\mathbf{H}_s + \mathbf{h}^m)\right] + \frac{\alpha}{|\mathbf{M}|}\left[\mathbf{M}\times\frac{d\mathbf{M}}{dt}\right] \tag{3.11}$$

In the above equation, γ is a gyromagnetic ratio, α is the phenomenological damping coefficient, and $\mathbf{h}^m$ is the AC component of the magnetic field inside the NP (see Figure 3.1b). The second term in this equation corresponds to the deceleration of this motion or, in other words, a damping effect. It involves energy loss from the motion of the magnetization field, which is converted to the heat energy in a ferromagnet [26]. The mechanism of transferring energy from one form to another is complex to describe in the field equations; that is why the damping parameter is introduced. It is determined experimentally for different materials. The damping constant may vary even for the same

material in different cases. The damping constant, α, for cobalt material, lies between 0.001 and 0.05 [58].

From the LLG equation, two characteristic functions, $\mu(\tilde{w})$ and $g(\tilde{w})$, were derived [27]. These two functions are permeability tensors of a ferromagnetic material in the x-y plane and z-direction, respectively:

$$\mu(\tilde{w}) = 1 + \tilde{w}_m \frac{1 + i\alpha\tilde{w}}{(1 + i\alpha\tilde{w})^2 - \tilde{w}^2} \quad , \tag{3.12}$$

$$g(\tilde{w}) = \frac{\tilde{w}_m \tilde{w}}{(1 + i\alpha\tilde{w})^2 - \tilde{w}^2} \, . \tag{3.13}$$

These expressions accounted for the derivation of the effective relative permeability of the medium [27]:

$$\mu_{eff}(\tilde{w}, \psi) = \left(1 + 3\psi \frac{\mu + g - 1}{\mu + g + 2} \right) , \tag{3.14}$$

where $\tilde{w}$ is applied frequency normalized by the natural precession frequency $w_r = \gamma\mu_0 \left| \boldsymbol{H}_{ex} \right|$, and $\tilde{w}_m = \gamma\mu_0 M / w_r$.

The resonance frequency is a frequency at which a composite captures the highest fraction of energy of the incident signal. In general, resonance frequency depends on the size, shape, and the composition of the material [59]. In our system, the resonance frequency, w_c, depends on (a) the magnitude of the external biased magnetic field, $\mathbf{H}_{ex}$, (b) magnetic properties of nanoparticles (magnetocrystalline anisotropy), and (c) the volume fraction of the nanoparticles within the composite. It can be calculated as [27]

$$w_c = \gamma\mu_0(|\boldsymbol{H}_{ex}| - \psi M_s + \frac{2K_1}{\mu_0 M_s}) . \tag{3.15}$$

This means that the resonance frequency depends linearly on the volume fraction of nanoparticles, ψ , which is no longer a constant value for the elastic matrix, undergoing deformations. As a resonance condition is fulfilled, the absorption of the EM wave significantly increases.

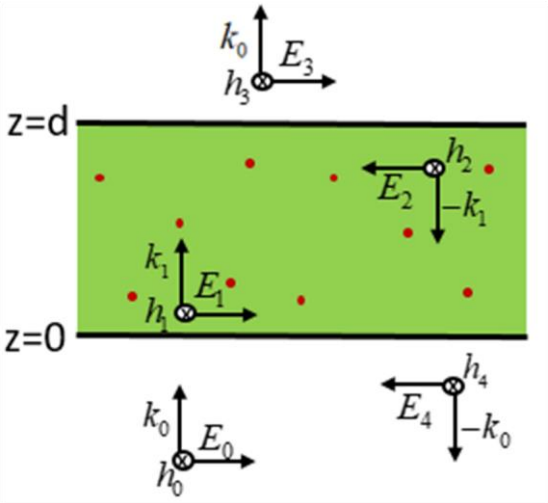

Figure 3.2: Graphical representation of the reflection and transmission of an incident EM wave traveling through the thin film. The wave vectors k_0 and k_1 denote two media: air and composite sample.

The analysis of the interaction between the microwave and composite film is based on the theory of electromagnetic waves in nonconducting media. By convention, we chose the normal incidence of the microwave. The incident wave ($\boldsymbol{E}_I = \boldsymbol{E}_0 e^{i(\boldsymbol{k}_1 z - wt)}$) gives rise to the reflected ($\boldsymbol{E}_R = \boldsymbol{E}_4 e^{i(-\boldsymbol{k}_2 z - wt)}$) and transmitted waves ($\boldsymbol{E}_T = \boldsymbol{E}_3 e^{i(\boldsymbol{k}_1 z - wt)}$), and some fraction of the incident power is absorbed. The wave that travels through the thickness of the film is subjected to specific boundary conditions. From electrodynamics we know four general

boundary conditions for the case of two linear media: *i)* $\varepsilon_1 E_{1\perp} = \varepsilon_2 E_{2\perp}$, *ii)* $B_{1\perp} = B_{2\perp}$, *iii)* $E_{1\|} = E_{2\|}$, *iv)* $\frac{1}{\mu_1} B_{1\|} = \frac{1}{\mu_2} B_{2\|}$ [60]. In our formulas we used the magnetic field $\boldsymbol{h}$ that is related to $\boldsymbol{B}$ through $\boldsymbol{h} = \boldsymbol{B} / \mu$. We considered that the electric and magnetic components of the wave is perpendicular to the external field (see Figure 4.2). The electric and magnetic field vectors were projected at two boundaries: z=0 and z=d as shown in Figure 4.2.

At the interfaces, the electric and magnetic components of the EM wave are parallel to the surface (boundary condition *iii*) and *iv)*), and can be written as [27]:

$$\begin{cases} E_0 - E_4 = E_1 - E_2 e^{-i\boldsymbol{k}_1 d} \\ h_0 + h_4 = h_1 + h_2 e^{-i\boldsymbol{k}_1 d} \end{cases} \quad (z = 0),$$
$$\begin{cases} E_1 e^{-i\boldsymbol{k}_1 d} - E_2 = E_3 \\ h_1 e^{-i\boldsymbol{k}_1 d} + h_2 = h_3 \end{cases} \quad (z = d). \tag{3.16}$$

Where $\boldsymbol{k}_1$ is a wave vector in the composite and can be expressed by the wave vector in free space, $k_0 = w\sqrt{\varepsilon_o \mu_0}$:

$$\boldsymbol{k}_1 = \boldsymbol{k}_0 \sqrt{\varepsilon_{eff}\, \mu_{eff}(w, \psi)} \tag{3.17}$$

The amplitudes of magnetic and electric fields are related through $\boldsymbol{h} = (\varepsilon / \mu)^{1/2} \boldsymbol{E}$; this expression helped to simplify the system of Equations 3.16 and to solve it for E .

The transmission coefficient, T , is defined as a ratio of an intensity transmitted to an intensity incident. The reflection coefficient, R , is the ratio of an intensity reflected to an intensity incident [60]. The intensity of the wave is the average of the Poynting vector

(energy per unit area, per unit time). The intensity of the incident, transmitted, and reflected wave are calculated as

$$< S_0 >= \frac{1}{2Z_0}\left|E_0\right|^2, < S_3 >= \frac{1}{2Z_0}\left|E_3 e^{-ik_1 d}\right|^2, < S_4 >= \frac{1}{2Z_0}\left|E_4\right|^2, \tag{3.18}$$

After E_3 and E_4 are expressed through E_0 , the simplified version of these coefficients are [27]:

$$T(\tilde{w},\psi) = \left\{\frac{4e^{-ik_1 d} Z(\tilde{w},\psi)}{(Z(\tilde{w},\psi)-1)^2 e^{-2ik_1 d} Z(\tilde{w},\psi) - (Z(\tilde{w},\psi)+1)^2}\right\}^2 \tag{3.19}$$

$$R(\tilde{w},\psi) = \left\{\frac{(Z(\tilde{w},\psi)^2 - 1)(e^{-2ik_1 d} - 1)}{(Z(\tilde{w},\psi)-1)^2 e^{-2ik_1 d} - (Z(\tilde{w},\psi)+1)^2}\right\}^2, \tag{3.20}$$

where Z_0 is the impedance of an EM wave in the vacuum and $Z(\tilde{w},\psi)$ is a ratio between the wave impedances in the composite and vacuum:

$$Z(\tilde{w},\psi) = \sqrt{\mu_{eff}(\tilde{w},\psi)/\varepsilon_{eff}} \ . \tag{3.21}$$

The impedance of an absorbing material, Z , can be modified by changing the type of polymer matrix [61], as well as type and concentration of NPs. The electric permittivity (ε_{eff}) and magnetic permeability (μ_{eff}) are parameters that define the dielectric and magnetic properties of materials and are directly associated to their absorbing characteristics. The absorption coefficient $\eta(\tilde{w},\psi)$ is defined as the ratio of the energy absorbed by the composite of the thickness, *d*, to the energy supplied into the system:

$$\eta = 1 - T(\tilde{w}, \psi) - R(\tilde{w}, \psi) . \tag{3.22}$$

This expression is based on the law of energy conservation, and the coefficients T and R are given by Equations 3.19-3.20. The energy that has been absorbed dissipates into heat. For convenience, this dissipated energy was measured as the incident power of the EM wave per unit area, P_0 (units W/m^2).

The temperature rise per unit time of the sample (heating rate) is equal to the ratio of the total energy absorbed by the sample per unit time ($P_0 \times \eta \times A$) to the total heat capacity ($c_p \times m, \quad m = \rho \times A \times d$) of the sample [27]:

$$K_T = \frac{P_0 \eta(\tilde{w}, \psi)}{\rho c_p d} \tag{3.23}$$

where, ρ is the density of the composite, c_p is a specific heat capacity and d is the thickness of the sample in the direction perpendicular to the incident EM wave.

The above framework introduces how to calculate an instantaneous heating rate if the volume fraction of nanoparticles, ψ , and the thickness of the gel layer, *d*, are two known instantaneous values. When the EM irradiation is applied, the thickness *d* and the volume fraction of the nanoparticles, ψ , vary with time as the sample is deformed due to heating. In our computational model, we have taken into account all these changes. Specifically, to capture the elastodynamics of composite within the M-gLSM framework, at each instant of time, we calculated (1) an instantaneous heating rate (Equation 3.23) with η from Equation 3.22 that depends on the gel thickness, *d*, and the volume fraction of the

nanoparticles, ψ , (2) an instantaneous temperature, *T*, of the sample based on this heating rate and temperature of the sample in the previous moment of time; and (3) a polymer-solvent interaction parameter that depends on temperature and defines the degree of swelling of the gel as given above, Equation 3.7; Lastly, in step (4), we performed an integration of the elastodynamics equations (3D gLSM) using this calculated polymer-solvent interaction parameter. As noted above, the nanoparticles are considered to be grafted to (or physically trapped within) the polymer matrix and they move together with the matrix. The volume fraction of nanoparticles, ψ , is calculated as $\xi_m \varphi$, where the parameter ξ_m sets the initial fraction of nanoparticles grafted onto the polymer matrix. We thus used our M-gLSM framework to account for the effects of interactions of the electromagnetic wave and the gel composite filled with ferromagnetic nanoparticles and for the coupling between magnetic heating and mechanical response of the gel matrix. For simplicity here we considered only small cubic gel samples freely suspended within the solvent; these samples represent a fraction of the thin uniform gel layer. An initial temperature of the system sets the equilibrium degree of the gel swelling (in the absence of an applied electromagnetic signal) and thereby sets the equilibrium dimensions of the sample [62].

3.3: The Relationship of Simulation Parameters to Experimental Values

In the simulations below, we choose the reference parameters based on the following available experimental values. The reference parameters for the

nanoparticles are chosen for the single domain cobalt (Co) nanoparticles taking the saturation magnetization and the magnetocrystalline anisotropy as $M_s = 1.44 \times 10^6 A/m$ and $K_1 = 4.5 \times 10^5 J/m^3$, respectively[27]. Hence, we use the following reference values: $w_m/2\pi = \gamma\mu_0 M_s/2\pi$ (taking the gyromagnetic ratio as $2 \times 10^{11} rad/Ts$ and the magnetic permeability of the vacuum as $\mu_0 \approx 1.257 \times 10^{-6} H/m$ and $w_r/2\pi = w_r^0/2\pi - w_m\psi/2\pi$, where $w_r^0/2\pi = \gamma\mu_0/2\pi(|\boldsymbol{H}_{ex}| + (2K_1/\mu_0 M_s) - M_s/3)$is independent on nanoparticles concentration). Taking $\mu_0|\boldsymbol{H}_{ex}|$=0.29T in the reference case, we set $w_r^0/2\pi$=10GHz. Note, that in the absence of the external field ($|\boldsymbol{H}_{ex}| = 0$), $w_r^0/2\pi = 0.68\ GHz$ (same as in Reference [27]).

Below we also consider dynamics of composites filled with iron oxide nanoparticles (magnetite, or Fe_3O_4). For these composites, we set $w_m/2\pi = 19.2\ GHz$, $M_s = 4.8 \times 10^5 A/m$, and H_a=0 (see Reference [27]). In this case, we consider two values of the external field, $\mu_0|\boldsymbol{H}_{ex}| = 0.3\ T$ and $\mu_0|\boldsymbol{H}_{ex}| = 0.5\ T$, setting $w_r^0/2\pi = 3.1 GHz$ and $w_r^0/2\pi = 9.6\ GHz$ for these external fields, respectively.

For the relative permittivity of a medium (PNIPAAm), we set $\varepsilon_{eff} = 70$ [63]. Notably, the variations in ε_{eff} remain small around the volume phase transition [63], so that these variations could be neglected. The phenomenological damping coefficient α is measured experimentally and typically ranges[58] from 0.001 to 0.05. Herein, following Reference [27], we set α=0.05.

For the properties of hydrogel matrix, we chose the volume fraction of polymer at preparation and the dimensionless crosslink density as $\varphi_0 = 0.114$ and, $c_0 v_0 = 7.2 \times 10^{-14}$, respectively [9]. For the gel-solvent interaction parameter, we set $\chi_1 = 0.518$ and calculated $\chi_0(T)$ as specified above (Equation 3.6) using $\delta h = -12.4 \times 10^{-14}$ and $\delta s = -4.7 \times 10^{-16}$ for the variations in the enthalpy and entropy per monomeric unit of the network based on the respective experimental data for neutral PNIPAAm gels [9]. We then calculate an equilibrium degree of swelling at $T^{ini} = 30^0 C$ as $\lambda^{ini} = 1.079$, and correspondingly, equilibrium polymer volume fraction, $\varphi^{ini} = 0.09$. We set an initial volume fraction of nanoparticles as $\psi^{ini} = \xi_m \varphi^{ini}$ by choosing the $\xi_m = 0.1$ in the reference case. Below, we also very (decrease) the initial volume fraction of the nanoparticles to probe the effects of their concentration on gels deformations driven by an application of an EM signal.

Taking the dimensionless units of length in our simulations to be $L_0 = 7 \times 10^{-7} m$, we can relate the initial dimensional thickness of the gel to the dimensional value of $d_0 = d^{ini} L_0 \approx 5.3$microns, where d^{ini}=$(L_z - 1)\lambda^{ini}$ is the initial dimensionless thickness of the sample, with the sample size taken as 8×8×8. The characteristic time scale can be estimated as [64] $\tau_0 \approx d_0^2/D$, where D is a collective diffusion coefficient for the polymer gel matrix. Choosing $D = 2 \times 10^{-11}\ m^2/s$[64] and relating the dimensional characteristic relaxation time for this sample to the dimensionless relaxation time, which we calculate from the simulations as $\tau \approx 4.0$,

we estimate the characteristic time scale [65] as T_0 =0.3s. The dimensionless angular frequency in the simulations below is scaled with $W_0 = 2\pi \times 10^9 Hz$.

Finally, to calculate the heating rate in Equation 3.23, we probe two values of the power density of the incident EM wave. For the majority of runs, we set $P_0 \approx 0.5\ kW/m^2$, which is twice lower than the value used in Reference [27] and lower than the power density of sunlight. This value, however, significantly exceeds power densities used in the wireless communication systems. In the separate simulation run, we also show that even using significantly lower power density, $P_0 \approx 10\ W/m^2$, results in the same behaviour but correspondingly scaled with time. We have chosen this specific low value of the power density since this is the maximum power density for the millimeter-wave signals for frequencies between 6-100GHz required by the Federal Communication Commission (FCC)[66]. Finally, for simplicity, we use specific heat capacity of water, c_p=4185.5*J/(kg·K)*; however, our additional simulations show that accounting for the contributions from both polymer and water to c_p as polymer volume fraction varies during phase transitions even further amplifies the heating rate. We take the density of the water-gel system as 10^3kg/m^3.

CHAPTER 4

RESULTS AND DISCUSSION

4.1 Dynamics of the Gel Composite Filled with Cobalt Nanoparticles

We now utilize the M-gLSM approach developed above to focus on the mechanical response of the gel composite under the influence of EM waves of different frequencies. Our first simulation run began with setting the external field of the electromagnet to $\mu_0|\boldsymbol{H}_{ex}|$=0.3T , and applying an AC signal with three different frequencies (Figure 4.1a) for a fixed duration of time (10^3 dimensionless time units, which is approximately equal to 5 minutes with the above scaling). These three dimensionless frequencies (w=26.7, w=27.4, w=32.0) have been chosen to show the distinct changes in the system. Initially all the samples are identical, with the volume fractions of nanoparticles set to $\psi = 9 \times 10^{-3}$. The snapshot (I) in Figure 4.1b shows the sample at the initial state; the colors in this figure represent different volume fractions of the polymer, φ, with the green corresponding to the lowest and the violet to the highest value of φ, respectively. For the applied dimensionless frequency w=32.0 and the time interval t=10^3, we observe nearly linear increase in the temperature (green line in Figure 4.1a). This correlates with the approximately constant value of the absorption coefficient, η, at this frequency (Figure 4.2a, green line), a small decrease in the sample thickness (green line in Figure 4.2b) and insignificant increase in the volume fraction of the nanoparticles (green line in Figure 4.2c). In this case, the response of gel-nanoparticle composite resembles, to some extent, the behavior of non-

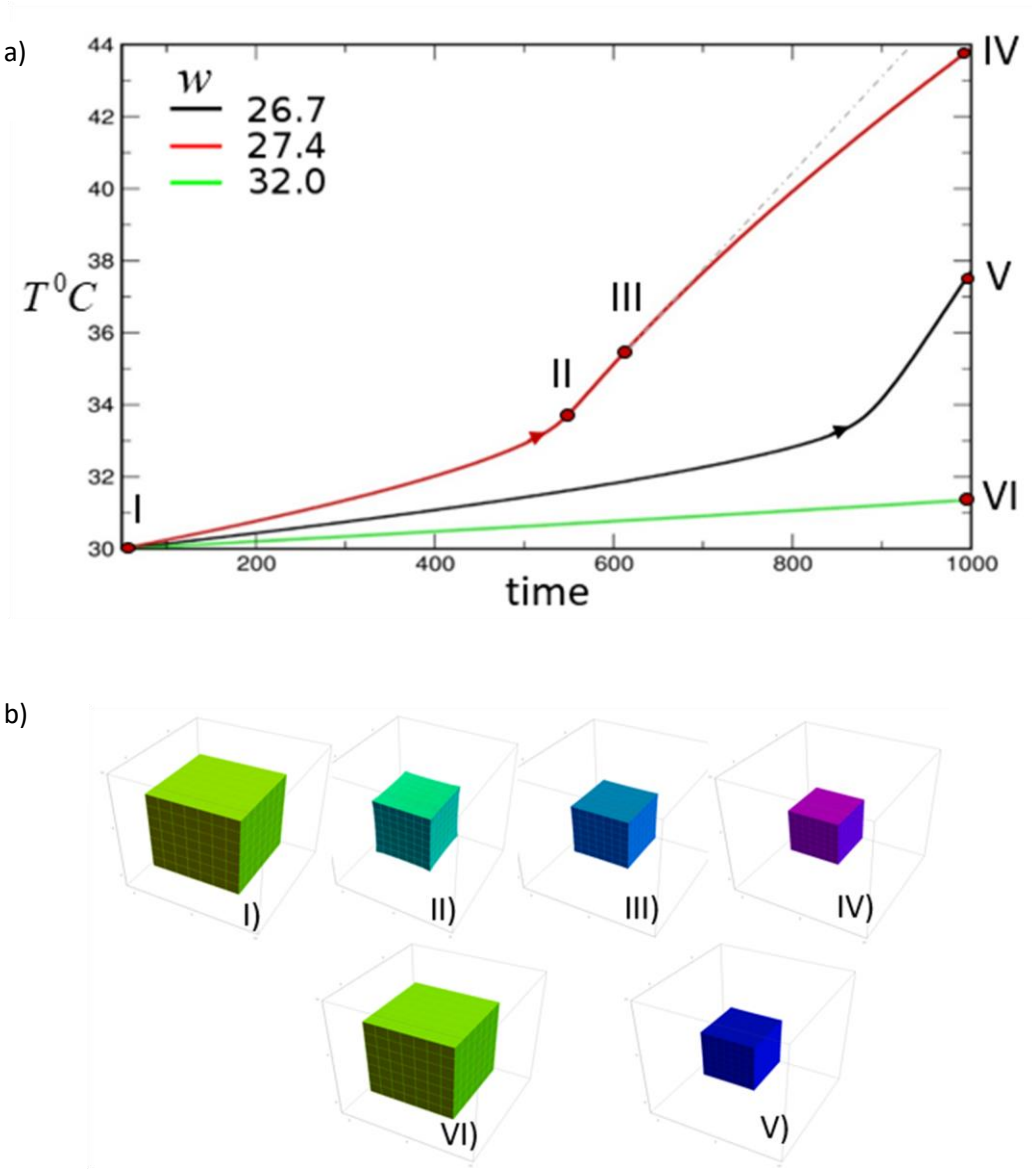

Figure 4.1: a) The FMR heating of the composite with the initial concentration of Co nanoparticles set at $\psi_{ini} = 9 \times 10^{-3}$ under normalized frequencies of an EM wave as given in the legend; **b)** Gel composites at different moments in time as marked with the corresponding symbols (I-VI) in a). The color here and in the following figures represents the volume fraction of the polymer, with the green corresponding to the lowest and the violet corresponding to the highest value of φ, respectively.

deformable composites [27] under FMR heating with the small deviations caused by the shrinking of the composite. For the two other frequencies (w=26.7, w=27.4) of the EM wave chosen in Figure 4.1a, we observed, in time, a sharp increase in the heating rate (remaining two curves in Figure 4.2), resulting in non-linear increase in temperature; an abrupt temperature change occurs at an earlier time for w = 27.4 (red curve) than for w = 26.7 (black curve). The snapshots in Figure 4.1b (I-IV) correspond to different times along the red curve in Figure 4.1a and clearly show that an application of the EM wave at this frequency results in the fastest shrinking of the sample. The three different frequencies considered here exhibit distinctly different rates of heating and, correspondingly, distinctly different degrees of swelling by the end of the simulation runs (at t = 10^3), as can be seen

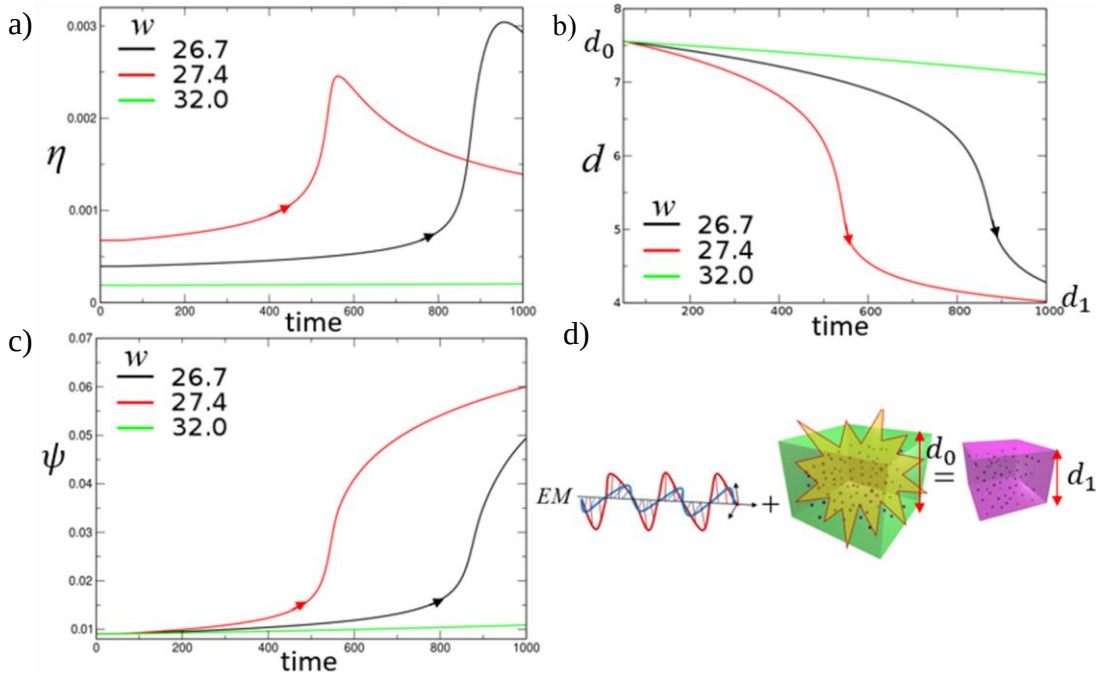

Figure 4.2: a) Absorption coefficient η as a function of time for the three normalized frequencies as given in the legend. **b)** Evolution of the thickness, d, for the simulation runs in a). **c)** The time evolution of the volume fraction of nanoparticles, ψ, for the same simulation runs. **d)** Schematic representation of the FMR heating in the gel composite.

by comparing the morphologies of the samples corresponding to the final snapshots in these simulations for the red, black, and green curves (see snapshots shown in Figures 4.1b IV, V and VI).

To understand the physical origin of the behavior observed in Figure 4.1a, we now plot the polymer volume fraction, φ, for the same simulation runs (see Figure 4.3). The red (w=27.4) and black curves (w=26.7) in Figure 4.3 show a distinct increase in φ at approximately t~500 and t~850 respectively (blue points). These two effective points show the identical pattern for the absorption coefficient and temperature, with the corresponding frequencies observed in Figure 4.2a and Figure 4.1a. However, at w=32.0 an increase in φ remains low and approximately linear within the considered simulation time frame (green line in Figure 4.1a). It is essential to remember here that the concentration of

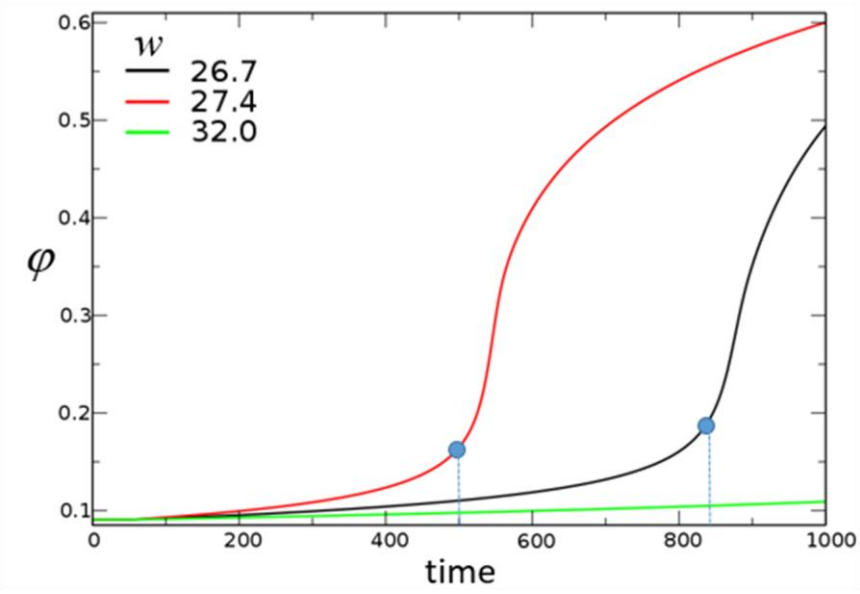

Figure 4.3: The time evolution of the volume fraction of the polymer, φ, for the same simulation runs as shown in Figure 4.1a and 4.2.

nanoparticles, ψ, is proportional to the polymer volume fraction, φ , and NPs move together with the matrix as a gel shrinks. As was described in Chapter 4, the coeficient of proportionality ξ_m=0.1 relates these two parameters as $\psi = \xi_m \varphi$.

In Figure 4.4a we plotted the data from the same simulations as in Figures. 4.1a 4.2 and 4.3 but now we have calculated a corresponding degree of swelling $\lambda(T)$ for each instant in time for all three cases (see Equation 3.7). The initial state of the sample is in swollen form (λ =1.08, green cubic sample). As expected for w=32.0 there was no significant change in volume, and the transition curve stopped not far from the original state (bold green dot). At frequency w=27.4 the sample underwent the complete phase transition (more than 60% of water was released) during the time period $t = 10^3$, reaching the shrunken state (violet cube). The black curve (w=26.7) reaches the bold black dot in the center, which corresponds to the VPT point in Figure 4.4b. From this we can say that an applied frequency defines the point on this curve that is reached during the fixed time interval. This plot illustrates that all the curves eventually will overlap, following the same volume phase transition curve if the radiation is held for a sufficient amount of time (the blue arrow shows the direction of time). Taking the first derivative of the complete transition curve (red one), we defined that the volume phase transition temperature is at 33.45^0C (see Figure 4.4b), corresponding to the reported values in literature for the PNIPAAm hydrogel [67].

After analyzing the above described physical processes in the composite, we returned to the description of the heating process in Figure 4.1a. The red curve exhibits a

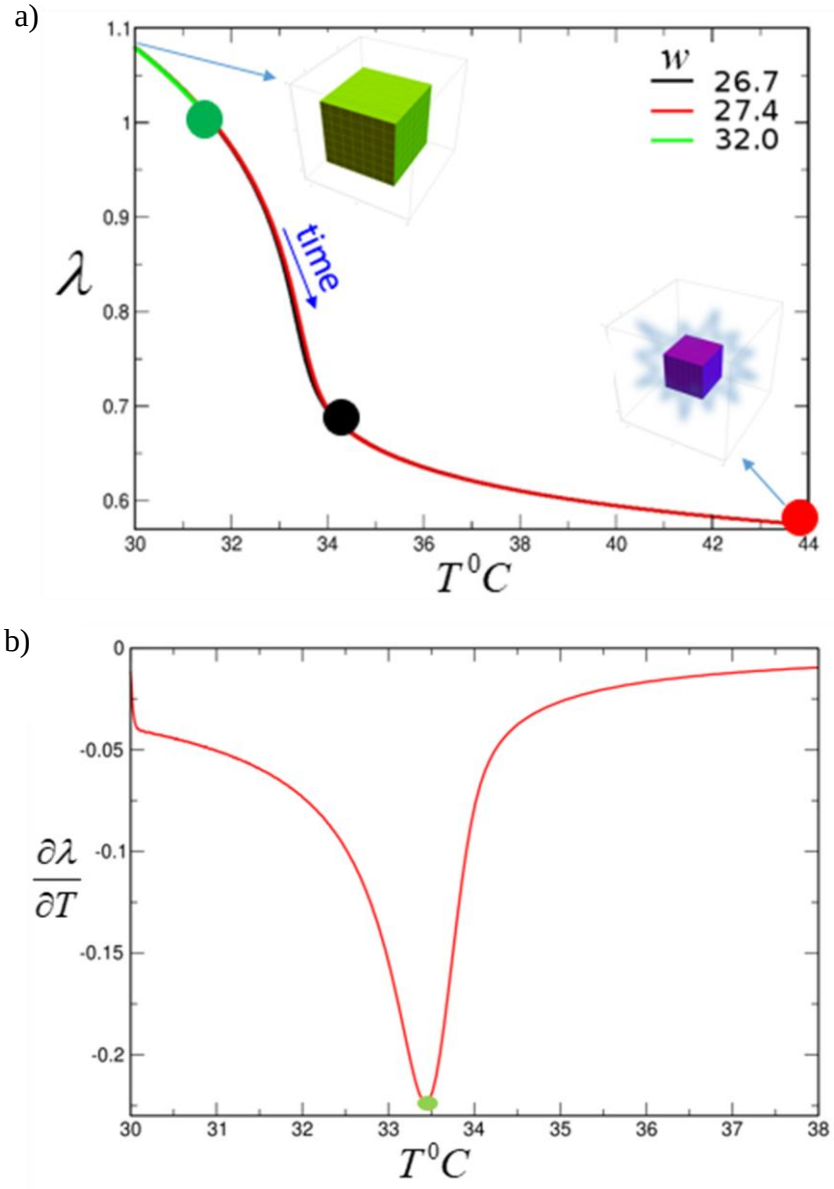

Figure 4.4 a) The degree of swelling of the gel-based composite, λ, as a function of its temperature at three different normalized frequencies as given in the legend. The blue arrow shows the direction of time, and the green, black, and red filled circles mark the points on the volume phase transition curve that are reached at a given applied frequency (w=32.0, w=26.7, w=27.4, respectively) after the signal was applied for a fixed duration of time ($t=10^3$); **b)** The first derivative of the volume phase transition curve as a function of T. The position of critical point (green dot) is at 33.45^0C.

steep increase in temperature upon shrinking close to the VPT due to an increase in the NP's concentration (as the gel samples continue to shrink, the nanoparticles draw closer to one another). However, this increase becomes less pronounced (the slope of the curve drops, marked by the dashed grey line) with an even further increase in concentration of NPs. In other words, we observe an amplification of the heating rate upon an increase in nanoparticles' concentration but only until this concentration reaches some critical value. This behaviour is clearly seen in corresponding time evolution plots of the absorption coefficient, η, (see red and black curves in Figure 4.2a) and the normalized value of η/d (see inset in Figure 4.5a).

To further investigate the amplification of the heating rate, we plotted η/d (red dots in Figure 4.5a) as a function of nanoparticles' concentration, ψ (the evolution of ψ during the same run is shown in Figure 4.2c, red curve). We note that η/d is more relevant in the characterization of the system's behaviour, since η/d has only a weak dependence on the thickness d, which could be neglected in the analysis, while η does depend on d strongly (see Figure 4.2a). As a result, η/d defines the heating rate (see Equation 3.23 above). The red dots in Figure 4.5a represent simulation data and the continuous black curve corresponds to the analytical expressions calculated using the above Equation 3.23 in the limiting cases, where d and ψ are chosen manually rather than taken from the simulations during the volume phase transitions.

An increase in the absorption coefficient with an increase in nanoparticles' concentration is anticipated, hence the drop observed in η/d at relatively high values of ψ in Figure 4.5a appears somewhat counterintuitive. To understand the origin of this

a)

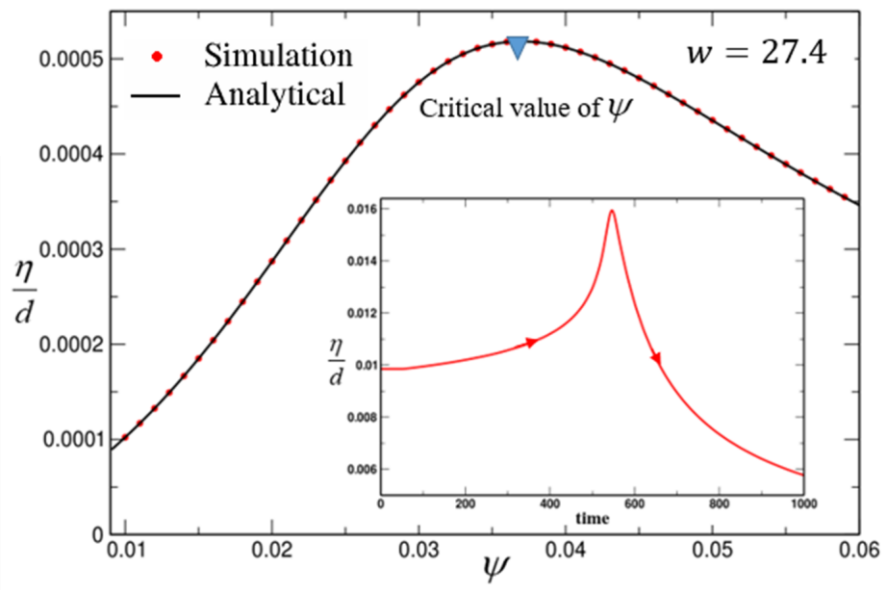

b)

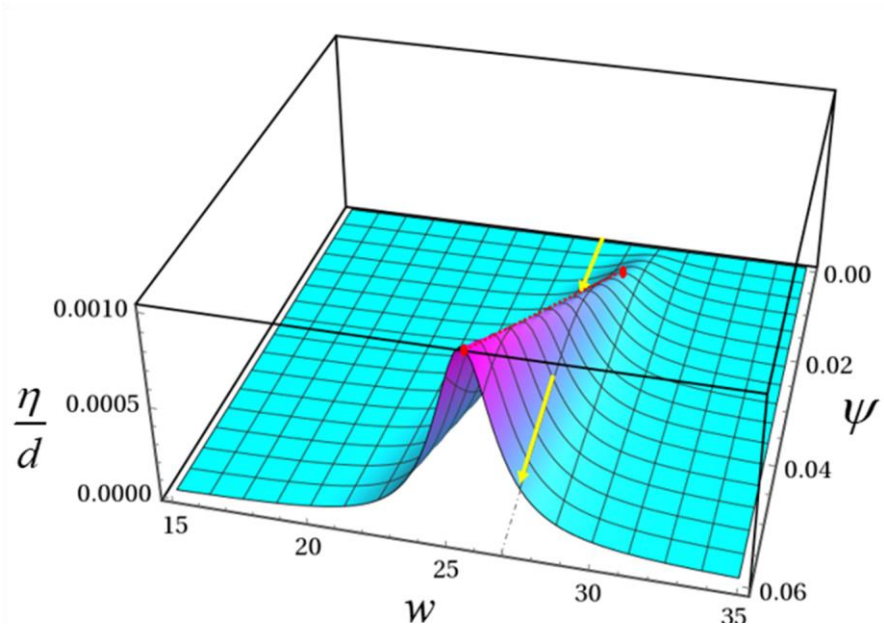

Figure 4.5 a) Absorption coefficient normalized by the thickness of the gel (η/d) as a function of volume fraction of nanoparticles, ψ, for w=27.4. The red dots represent simulation data, and the continuous black curve corresponds to the analytical calculations. The inset shows η/d from the same simulation run as a function of time; **b)** Surface plot of η/d as a function of the incident normalized frequency, w, and volume fraction of nanoparticles, ψ. The cross-section of the surface plot taken at w=27.4 (marked by the yellow arrows) represents the solid black curve in Figure 4.5(a).

behavior, we represented η/d as a 3D surface plot (Figure 4.5b), as a function of the frequency of the applied signal, w, and NPs' concentration, ψ, using the Equation 3.23. The resonance frequency is higher for the low concentrations of nanoparticles and linearly decreases with an increase in ψ (the peak shifts to the left at higher ψ in the three-dimensional surface plot in Figure 4.5b. If we follow the maximum peak values of η/d along the surface plot in Figure 4.5b by changing the frequency of an incident EM signal, w, to stay at the resonance frequency at any given concentration of ψ, the highest absorption are observed at the critical value of ψ. In other words, the height of the peak in Figure 4.5b increases with the increase in ψ with the corresponding variation in w to stay at the resonance frequency for each value of ψ. If, on the other hand, we fix the value of w (w is a constant) and follow the yellow arrow in Figure 4.5b, we find that the height of the peak first increases then decreases identically to the behavior observed in our simulations. The continuous black curve in Figure 4.5a represents the cross-section of the surface plot in Figure 4.5b taken at w=27.4 (analytical calculations); an overlap between the simulation results (red dots) and an analytical curve (continuous black curve) confirms the numerical accuracy of the integrating electrodynamic equations (given in the section 3.2) using M-gLSM.

In the next simulation runs, we characterized the sample temperature, T, and the effect of mechanical feedback through its thickness, d, by applying alternating electromagnetic fields at a range of frequencies for the given duration of time $t=10^3$. The blue curves in Figures 4.6a and 4.6b represent the final temperature and thickness of the sample for these frequencies at $t=10^3$, while black and red curves

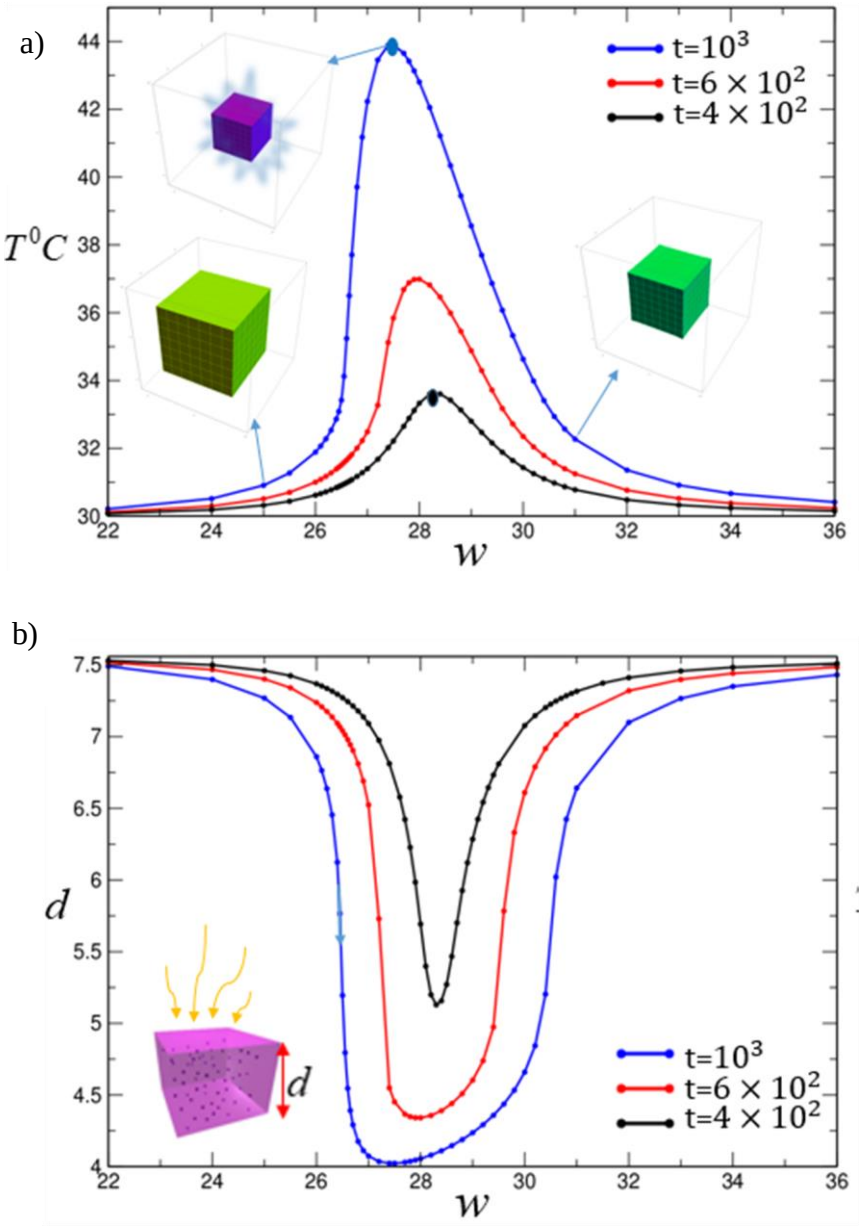

Figure 4.6: a) Temperature as a function of an applied frequency, *w*, for the duration of FMR heating t=4×10^2 (black curve), 6×10^2 (red curve) and 10^3 (blue curve). The images in the inset show composites at the time instances as marked by the arrows. **b)** The thickness of the sample as a function of an applied frequency, w, for the simulation runs in a).

correspond to sample's temperature at earlier times as shown in the legend. Note that at the frequency $w = 27.4$ selected in one of the examples in Figure 4.1a, the highest temperature is reached during this time interval. The temperature of the sample decreases with either an increase or a decrease in frequency with respect to the critical frequency at a given time, with the negligibly small heating for the frequencies significantly higher or lower than this value.

We underline the asymmetric nature of the bell-shaped curve in Figure 4.6a (blue curve), that can be inferred from Equation 3.15, which corresponds to the value of the resonance frequency, w_c. As the system undergoes volume phase transition, an increase of the volume fraction of the nanoparticles (proportional to the volume fraction of the polymer) causes a decrease of the resonance frequency with time (see a surface plot in Figure 4.5b and Equation 3.15). Therefore, the resonance frequency, w_c, is a variable and not a constant value, depending on the degree of swelling of the sample. Correspondingly, during early times, as long as shrinking is relatively insignificant (black curve in Figure 4.6a), the bell-shaped curve is nearly symmetric. The resonance frequency for this case (earlier times) is higher than that at later times. Notably, the sample's temperature, measured at a given time, accounts for the contributions of the temperature increments during the entire heating process as the sample undergoes volume phase transition.

Interestingly, our results show different feedback mechanisms in these composites. For a wide range of system parameters, positive feedback mechanism dominates: magnetic heating increases volume fraction of nanoparticles via gel shrinking, and this behavior, correspondingly, accelerates the rate of heat transfer in the gel-base composite. However,

a negative feedback mechanism also takes place: at some conditions, magnetic heating increases volume fraction of nanoparticles via gel shrinking beyond some peak value of ψ. The EM wave frequency in these cases is shifted significantly from the resonance frequency so that the further increase in ψ leads to the decrease in the heating rate (Figure 4.6).

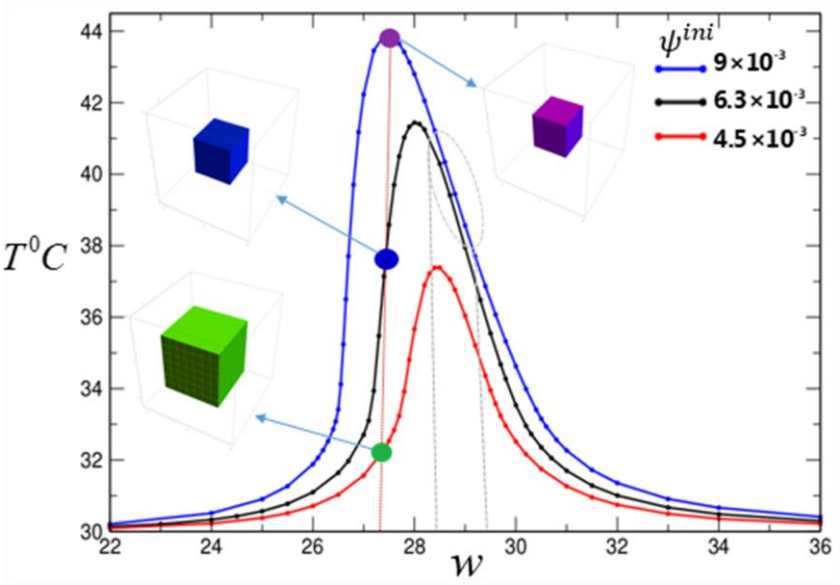

Figure 4.7: The temperature of the composite as a function of an applied frequency, *w*, for the dimensionless duration of FMR heating (t=10^3) at different initial volume fractions of nanoparticles: $\psi_{ini} = 9 \times 10^{-3}$ (blue curve), 6.3×10^{-3} (black curve), and 4.5×10^{-3} (red curve). The images in the inset show the composites at the frequency *w*=27.4.

In the next series of simulations (Figure 4.7), we varied the initial volume fraction of nanoparticles from $4.5\text{x}10^{-3}$(red curve) to $6.3\text{x}10^{-3}$ (black curve) to $9\text{x}10^{-3}$ (blue curve, our reference case). The plot in Figure 4.7 shows that, as could be anticipated from Equation 3.15, the peak value in the sample's temperature for the highest concentration of nanoparticles, ψ, (blue curve), is located at the lowest frequency (compared to that for the remaining values of NPs concentrations). The asymmetry of the bell-shaped curves can

again be understood from Equation 3.15 that allows us to determine the apparent critical frequency. Note the existence of a range of frequencies at which an application of a signal for this time interval shows distinctly different sample temperatures for different initial concentrations of nanoparticles (one such example is indicated by vertical red dashed line at $w = 27.4$ in Figure 4.7). However, at certain values of applied *w*, the heating and, correspondingly, the mechanical response would be similar for the samples with different volume fractions of nanoparticles (see nearly overlapping regions on the blue and black curves, highlighted in grey dashed oval in Figure 4.7). The nonlinear effects discussed above are the cause of these closely matching responses for different samples.

In the next series of simulations we examined the thermomechanical properties of the composite that has confined boundaries, comparing it with the reference (free) case. Under the same conditions, the magnetic heating, and, as a result, the rate of the heat transfer, is more pronounced for the free case (blue curve) than for the confined (black curve with green dots in Figure 4.8). This could be explained based on the fact that the movement of polymer chains are restrained and the volume fraction of NPs doesn't change significantly. Consequently, the chain conformation is unable to make a large-scale elastic deformation**.** However, magnetic heating raises the temperature of the composite approximately to 37^0C. The insets represent the volume fraction of the composite at maximum absorption (resonance condition); confined composite is identical to the initial state of the reference sample (see Figure 4.1) and the response of this systems closely resemble the response of the non-elastic composite (paraffin film with magnetic nanoparticles).

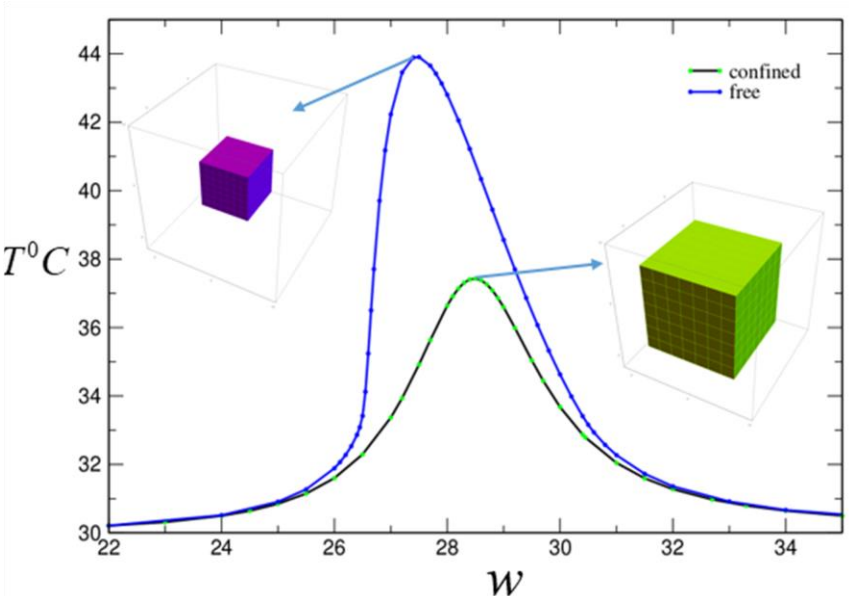

Figure 4.8: Temperature as a function of applied frequency, *w*, of the confined composite (black curve with green dots) and the composite of the free boundaries (blue curve) under the same conditions: concentration of nanoparticles ($\psi = 9 \times 10^{-3}$), the strength of the applied signal ($P_0 = 0.5\ kW/m^2$), and the dimensionless irradiation time ($t=10^3$).

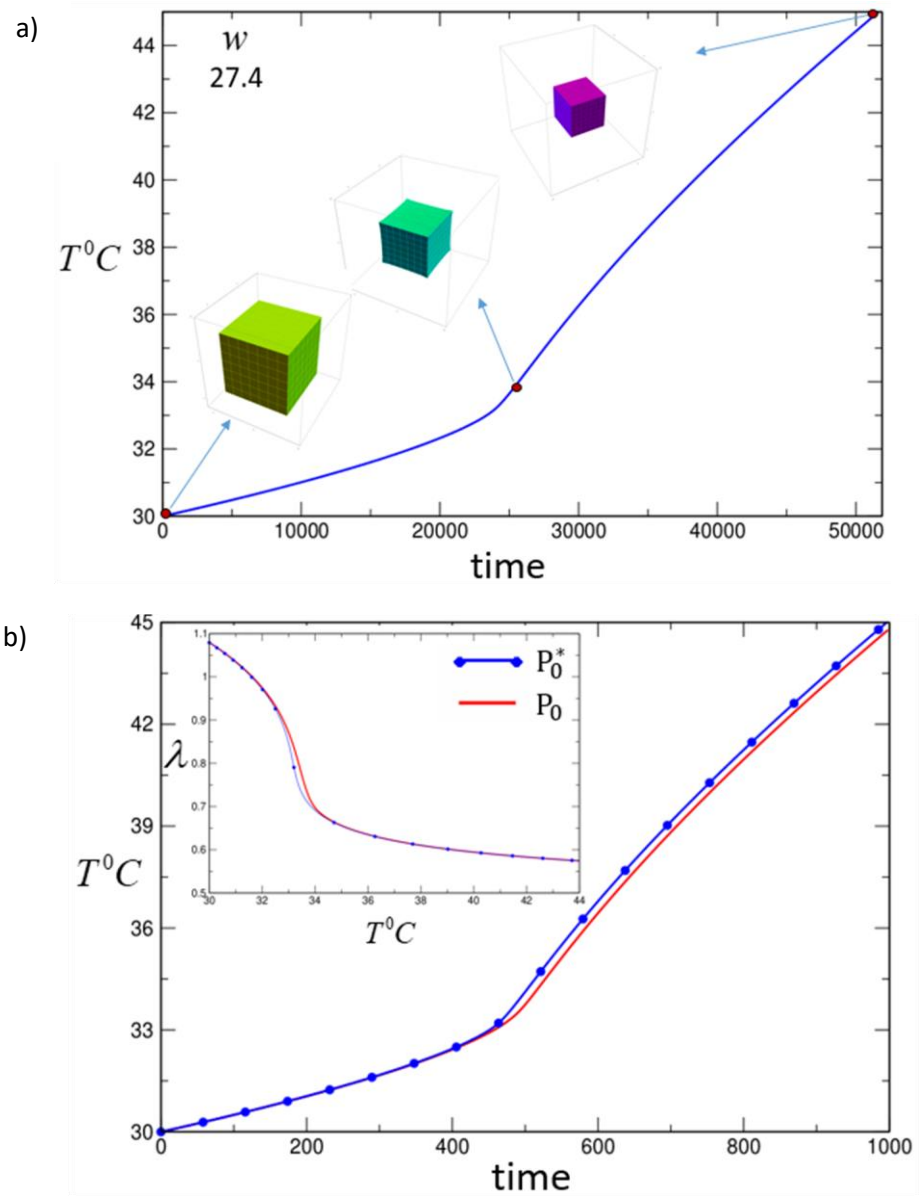

Figure 4.9: a) The FMR heating at the reduced power density, corresponding to P_0^*=9.988 W/m^2. The rest of the simulation parameters are the same as in Figure 4.1a (red curve). **b)** Both curves (the red curve in Figure 4.1a and the curve in a) overlap if the time in a) is scaled by P_0/P_0^*=51.81, where P_0=517.50 W/m^2 (the reference value of the power density in our system). The inset shows the same scaling for these two values of P_0 for the degree of swelling λ as a function of temperature. The red curves represent the simulation data of the reference case, and the blue dotted curves corresponds to the data in a) with the time scaled by P_0/P_0^*.

In the last series of simulations for the composite filled with cobalt NPs we studied the FMR heating at the reduced power density, corresponding to $P_0^* \approx 10$ W/m^2. The rest of the parameters are the same as in the simulations run, shown in Figure 4.1a (the red curve). As shown in the Figure 4.9a, the system takes a relatively longer time to reach the exact heating effect ($\sim 44^0$C) as at the power density $P_0 \approx 0.5$ kW/m^2 (the reference value in our system). Figure 4.9b demonstrates that for the same two runs, both curves (blue curve in Figure 4.1a and the curve in 4.9a) overlap if the time in 4.9a is scaled by P_0/P_0^*, since the heating rate is proportional to the power density. The inset shows the same scaling for these two values of P_0 for the degree of swelling λ as a function of temperature. Here, the red curves correspond to the simulation in Figure 4.1a, and the blue dotted curves represent the data in the Figure 4.9a with the time scaled by P_0/P_0^*.

4.2: Dynamics of Gel Composite Filled with the Fe_3O_4 Nanoparticles

As was described in Chapter 2, superparamagnetic nanoparticles Fe_3O_4 have gained extensive attention because of their relevance for many applications, such as a contrast agent in Magnetic Resonance Imaging (MRI), drug delivery, hypothermia treatment, and magnetic recording [68]. Because magnetite nanoparticles are found in living organisms, they are considered biocompatible and environmentally friendly. The well-studied example is magnetotatic bacteria that synthesizes nanosized magnetic granules (magnetosomes) [69], which function as tiny compasses that allow bacteria to migrate along earth field lines. Nanosized magnets have also been found in other living beings: some birds, insects and fish [70].

In the above chapter we already demonstrated the sufficient heat generation by the cobalt nanoparticles that results in a significant deformation of the gel matrix. Then we compared the results of the FMR heating with the one for Fe_3O_4 nanoparticles at the same conditions. In Figure 4.10a, we focused on the response of the composite with the fixed initial concentration of nanoparticles ($9x10^{-3}$) placed into the external fields of $\mu_0 |\mathbf{H}_{ex}| = 0.3\text{T}$ (black curve) and $\mu_0 |\mathbf{H}_{ex}| = 0.5\text{T}$ (blue curve). The remaining modeling parameters are provided in section 3.3 above. As can be anticipated from Equation 3.15, the resonance frequency is shifted towards the right in a higher external field. Again, similar to the simulations shown in Figure 4.6a, we kept the AC EM signal on for the same duration of time (10^3 dimensionless units, corresponding to 5 minutes with the scaling given in section 4.2). The heating rate in these iron oxide nanoparticles, however, is significantly lower [27] than in Co nanoparticles. Hence, our simulations show that this time interval is not sufficient to drive the sample through the volume phase transitions (the VPT of our PNIPAAm gel is at $T=33.45^0C$ (see Figure 4.4b), and heating from Fe_3O_4 nanoparticles reached $T=33.19^0C$,). We also note the symmetry of the bell-shaped curves in Figure 4.10a: again, this is due to the relatively small degree of shrinking of the sample and, correspondingly, small increases in nanoparticles' volume fractions. Upon an application of the EM signal during the double time interval (the red line in Figure 4.10b), the sample undergoes volume phase transitions and the asymmetry of the bell-shaped curve becomes apparent with the resonance frequency

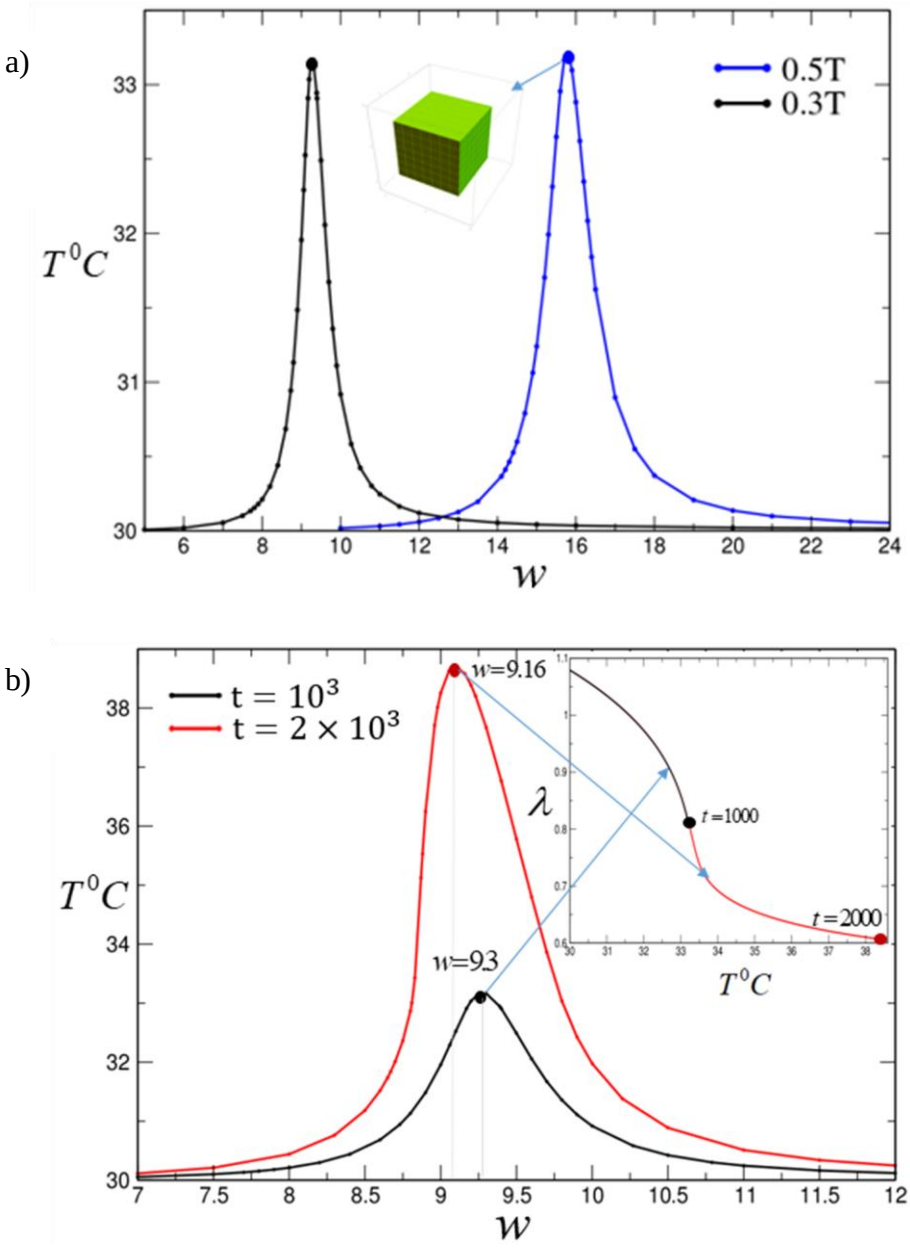

Figure 4.10: a) The temperature of the PNIPAAm-Fe_3O_4 composite as a function of an applied frequency, w, for the dimensionless time of FMR heating (t=10^3) at a volume fractions of nanoparticles $\psi_{ini} = 9 \times 10^{-3}$ and at $\mu_0|\mathbf{H}_{ex}|$=0.3T (black curve) and $\mu_0|\mathbf{H}_{ex}|$=0.5T (blue curve). **b)** The temperature as a function of an applied frequency, w, for the dimensionless time of heating t=10^3 (blue curve) and a t=2 x 10^3 (red curve) at $\mu_0|\mathbf{H}_{ex}|$=0.3T. **The inset**: the black circle on the black curve represents the degree of swelling at the corresponding resonance frequency (w = 9.3) at the time t=10^3, and the red circle on the red curve corresponds to the degree of swelling at the resonance frequency (w = 9.16) at the time t=2×10^3.

shifted to the left as in the previous scenario with Co nanoparticles. These results show that the observed behavior is robust and is observed for various types of nanoparticles.

In conclusion, we observed a more pronounced heating effect (as a result of shrinking) of the composite filled with cobalt NPs than of the composite filled with Fe_3O_4 NPs; the significant difference between these two performances could be explained from the magnetic properties of the cobalt NPs (high saturation magnetization and anisotropy).

CHAPTER 5

5.1 CONCLUSIONS

The objective of this study was to investigate the influence of FMR heating on the magnetic gel composite via theoretical and computational modeling. For this, we performed the following steps: 1) we proposed a model that accounts for the dynamic coupling between the elastodynamics of polymer gel and an FMR heating of magnetic nanoparticles; 2) through simulations we probed the system's behavior under the different conditions; 3) we evaluated and analyzed data.

In our work we focused on thermo-responsive hydrogel filled with uniformly dispersed magnetic nanoparticles that are covalently bonded or trapped within the polymer matrix. To model this system, we used an already-existing gLSM framework that captures gel elastodynamics [32]. We expanded it to account for the FMR heating [27] of the gel composite; we now refer to this model as M-gLSM model. During the application of the EM irradiation, the size of the sample and the volume fraction of the nanoparticles vary with time as the sample shrinks due to the heating; correspondingly, the heating rate as well as magnetic permeability changes dynamically, which is accounted for in our model.

Our results demonstrate that the heating rate is highly selective to the frequency of the incident EM signal and is nonlinearly coupled with the gel's elastodynamics. We observed a large-scale deformation of these gel composites in response to the relatively small variation of an applied EM signal within the GHz frequencies range. The resonance frequency, w_c, in our system depends on the type and concentrations of nanoparticles and

is a variable and not a constant value. This can clearly be seen in our results, when at the early stages of the FMR heating, the sample's temperature as a function of an incident frequency is a nearly symmetric bell-shaped curve with the maximum at a resonance frequency. At later times, however, as the shrinking of the sample becomes more pronounced, the resonance frequency shifts towards the lower values, so that the bell-shaped curve with the maximum at a resonance frequency becomes asymmetric.

Two distinct feedback mechanisms (positive and negative) are observed in these composites. For a set of parameters, positive feedback mechanism dominates: magnetic heating increases volume fraction of nanoparticles via gel shrinking, correspondingly increasing the heating rate. However, a negative feedback mechanism is also observed when magnetic heating increases the volume fraction of nanoparticles via gel shrinking beyond a critical value of volume fraction of nanoparticles (peak in Figure 5.5b), lowering the resonance frequency to achieve the maximum heating rate. Furthermore, one can tailor the system's response by varying either initial volume fraction of nanoparticles, a magnitude of the external bias field, or a frequency of the applied signal. We showed that varying initial volume fraction of nanoparticles results in distinctly different magnitude of the mechanical response of the composite.

In this study we considered two types of magnetic nanoparticles uniformly embedded into the polymer matrix: cobalt and iron oxide (magnetite) nanoparticles. Magnetite nanoparticles have a number of advantages because they are inexpensive, biocompatible, and have a good colloidal stability [38]; these nanoparticles are widely used

in different applications from MRI imaging to magnetic recording [68]. Cobalt NPs have high magnetization and hence generate heat efficiently [27].

We have shown that the main features of the system's mechanical response (high selectivity to the frequency of the applied signal and a shift towards lower values of resonance frequencies as the gel undergoes VPT) remain qualitatively the same for both types of nanoparticles, while the actual magnitude of the observed heating effect depend strongly on the chemical nature of the nanoparticles. Another method to tailor the composite's response is by varying a chemical nature of nanoparticles or by using a mixture of magnetic nanoparticles. Furthermore, while in our studies we chose PNIPAAm gels as a reference system, we expect that similar mechanical response will be observed for a range of thermoresponsive hydrogels [71] loaded with magnetic nanoparticles, for example for Poloxamer hydrogels. Poloxamer (commercial name Pluronics) is a tri-block copolymer, having a lower critical solution temperature (LCST) that depends on molecular weight and the ratio between these copolymers [3]. One of the main advantages of this hydrogel is the possibility to achieve any transition point (even the same as PNIPAAm) by varying the concentration of poloxamer and other excipients.

In summary, our results show that the interactions of an electromagnetic wave with the magnetic gel composites drive the volume phase transitions and result in large-scale mechanical responses of the samples for a range of applied frequencies and over a range of timescales. This response depends on the initial concentration of nanoparticles and their chemical nature and can be regulated dynamically by changing the intensity of the incident radiation, the irradiation time, or an external bias field. We demonstrated that these

composites exhibit high selectivity to the frequency of the incident EM signal. Our results suggest a new approach to encourage the design of active gel-based composites that could be used in a range of soft actuators remotely controlled by the low power EM signals within the GHz frequency range.

5.2: FUTURE WORK

In the above studies, we focused our attention on the small cubic samples; this geometry represents an ideal reference case for the studies of coupling between mechanical feedback and selective FMR heating in these composites. The developed M-gLSM framework readily allows one to account for the magnetic heating and non-uniform deformations of the spatially extended samples, and this is one of the objective of the future studies. In addition, the following corrections and improvements can be made to our magneto-elastic model to be able to capture wider range of system parameters:

- Introduce and estimate the required cooling of the system, so that these hydrogels could exhibit reversible thermo-responsive behavior.
- Investigate how different types and sizes of nanoparticles will affect the surface topology of the hydrogel.
- Account for the contributions from the dielectric losses for spatially extended samples, so it would be possible to capture the EM heating for a range of composites beyond the conditions considered in the above simulations.

Therefore, taking into account the above concepts could yield results that might lead to an even better understanding of the control of the heating rate in similar hydrogel-based systems.

REFERENCES

1. Chen, J.K. and C.J. Chang, *Fabrications and Applications of Stimulus-Responsive Polymer Films and Patterns on Surfaces: A Review.* Materials (Basel), 2014. **7**(2): p. 805-875.
2. Memic, A., et al., *Hydrogels 2.0: improved properties with nanomaterial composites for biomedical applications.* Biomed Mater, 2015. **11**(1): p. 014104.
3. Jalili, N.A., M. Muscarello, and A.K. Gaharwar, *Nanoengineered thermoresponsive magnetic hydrogels for biomedical applications.* Bioengineering & Translational Medicine, 2016. **1**(3): p. 297-305.
4. Meenach, S.A., et al., *Biocompatibility analysis of magnetic hydrogel nanocomposites based on poly(N-isopropylacrylamide) and iron oxide.* J Biomed Mater Res A, 2009. **91**(3): p. 903-9.
5. Satarkar, N.S. and J.Z. Hilt, *Magnetic hydrogel nanocomposites for remote controlled pulsatile drug release.* J Control Release, 2008. **130**(3): p. 246-51.
6. Sun, Y., et al., *Highly magnetic sensitivity of polymer nanocomposite hydrogels based on magnetic nanoparticles.* Composites Science and Technology, 2017. **141**: p. 40-47.
7. Philippova, O., et al., *Magnetic polymer beads: Recent trends and developments in synthetic design and applications.* European Polymer Journal, 2011. **47**(4): p. 542-559.
8. Palak P. Parikh, S.M., IEEE, Mitalkumar. G. Kanabar, , *Opportunities and Challenges of Wireless Communication Technologies for Smart Grid Applications* 2010.
9. Hirotsu, S., *Softening of bulk modulus and negative Poisson's ratio near the volume phase transition of polymer gels.* The Journal of Chemical Physics, 1991. **94**(5): p. 3949-3957.
10. Weeber, R., et al., *Polymer architecture of magnetic gels: a review.* J Phys Condens Matter, 2018. **30**(6): p. 063002.
11. Silva, V.A.J., et al., *Synthesis and characterization of Fe3O4 nanoparticles coated with fucan polysaccharides.* Journal of Magnetism and Magnetic Materials, 2013. **343**: p. 138-143.
12. Kita, E., et al., *Ferromagnetic nanoparticles for magnetic hyperthermia and thermoablation therapy.* Journal of Physics D: Applied Physics, 2010. **43**(47).
13. Campbell, S., D. Maitland, and T. Hoare, *Enhanced Pulsatile Drug Release from Injectable Magnetic Hydrogels with Embedded Thermosensitive Microgels.* ACS Macro Letters, 2015. **4**(3): p. 312-316.
14. Campbell, S.B., M. Patenaude, and T. Hoare, *Injectable superparamagnets: highly elastic and degradable poly(N-isopropylacrylamide)-superparamagnetic iron oxide nanoparticle (SPION) composite hydrogels.* Biomacromolecules, 2013. **14**(3): p. 644-53.
15. Reyes-Ortega, F., et al., *Magnetic Nanoparticles Coated with a Thermosensitive Polymer with Hyperthermia Properties.* Polymers, 2017. **10**(1).
16. Seki, A., et al., *Study of the heating characteristics and mechanisms of magnetic nanoparticles over a wide range of frequencies and amplitudes of an alternating magnetic field.* Journal of Physics: Conference Series, 2014. **521**.
17. Tong, S., et al., *Size-Dependent Heating of Magnetic Iron Oxide Nanoparticles.* ACS Nano, 2017. **11**(7): p. 6808-6816.

18. Kolhatkar, A.G., et al., *Tuning the magnetic properties of nanoparticles.* Int J Mol Sci, 2013. **14**(8): p. 15977-6009.
19. Pearce, J., et al., *Magnetic Heating of Nanoparticles: The Importance of Particle Clustering to Achieve Therapeutic Temperatures.* J Nanotechnol Eng Med, 2013. **4**(1): p. 110071-1100714.
20. Häring, M., et al., *Magnetic Gel Composites for Hyperthermia Cancer Therapy.* Gels, 2015. **1**(2): p. 135-161.
21. Zhang, Z.Q. and S.C. Song, *Thermosensitive/superparamagnetic iron oxide nanoparticle-loaded nanocapsule hydrogels for multiple cancer hyperthermia.* Biomaterials, 2016. **106**: p. 13-23.
22. Lin, X., R. Huang, and M. Ulbricht, *Novel magneto-responsive membrane for remote control switchable molecular sieving.* J. Mater. Chem. B, 2016. **4**(5): p. 867-879.
23. Ang, K.L., S. Venkatraman, and R.V. Ramanujan, *Magnetic PNIPA hydrogels for hyperthermia applications in cancer therapy.* Materials Science and Engineering: C, 2007. **27**(3): p. 347-351.
24. Jaiswal, M.K., et al., *Thermal behavior of magnetically modalized poly(N-isopropylacrylamide)-chitosan based nanohydrogel.* Colloids Surf B Biointerfaces, 2010. **81**(1): p. 185-94.
25. R. Herna´ndez, † J. Sacrista´n,† L. Ası´n,‡,§ T. E. Torres,‡,§ M. R. Ibarra,‡,§ G. F. Goya,‡,§ and and C. Mijangos†, *Magnetic Hydrogels Derived from Polysaccharides with Improved Specific Power Absorption: Potential Devices for Remotely Triggered Drug Delivery.* Journal of Physical Chemistry, 2010. **114**: p. 12002–12007.
26. Gilbert, T.L., *Classics in Magnetics A Phenomenological Theory of Damping in Ferromagnetic Materials.* IEEE Transactions on Magnetics, 2004. **40**(6): p. 3443-3449.
27. Gu, Y. and K.G. Kornev, *Magnonics: Selective heat production in nanocomposites with different magnetic nanoparticles.* Journal of Applied Physics, 2016. **119**(9): p. 095106.
28. Arbe, A., et al., *Dielectric Susceptibility of Liquid Water: Microscopic Insights from Coherent and Incoherent Neutron Scattering.* Phys Rev Lett, 2016. **117**(18): p. 185501.
29. Pearce, J.A., et al., *FEM numerical model study of heating in magnetic nanoparticles.* Proc SPIE Int Soc Opt Eng, 2011. **7901**.
30. John A. Pearce, J.R.C., Stanislav Y. Emelianov, *Ferrimagnetic Nanoparticles enhance microwave heating for tumor.* IEEE, 2010.
31. Landau, L.D. and E.M. Lifshitz, *Electrodynamics of continuous media*. 2nd ed. 1984, Oxford, New York,: Pergamon Press. 417 p.
32. Kuksenok, O., V.V. Yashin, and A.C. Balazs, *Three-dimensional model for chemoresponsive polymer gels undergoing the Belousov-Zhabotinsky reaction.* Phys Rev E Stat Nonlin Soft Matter Phys, 2008. **78**(4 Pt 1): p. 041406.
33. Suzuki, A. and T. Tanaka, *Phase-Transition in Polymer Gels Induced by Visible-Light.* Nature, 1990. **346**(6282): p. 345-347.
34. Guimaraes, A.P., *Principles of Nanomagnetism.* Springer Heidelberg Dordrecht London New York, 2009.
35. Fermon, C. and M.V. Voorde, *Nanomagnetism. Applications and perspectives.* Wiley-VCH Verlag GmbH & Co. KGaA, Boschstr. 12, 69469 Weinheim, Germany, 2017.

36. Feynmam, R., *The Feynman Lectures on Physics Vol II,Ch.34: The Magnetism of Matter.* 2006.
37. Coey, J.M.D., *Magnetizm and magnetic materials.* (Cambridge University Press,Cambridge), 2010.
38. Obaidat, I.M., B. Issa, and Y. Haik, *Magnetic Properties of Magnetic Nanoparticles for Efficient Hyperthermia.* Nanomaterials (Basel), 2015. **5**(1): p. 63-89.
39. Akbarzadeh, A., M. Samiei, and S. Davaran, *Magnetic nanoparticles: preparation, physical properties, and applications in biomedicine.* Nanoscale Res Lett, 2012. **7**(1): p. 144.
40. Kudr, J., et al., *Magnetic Nanoparticles: From Design and Synthesis to Real World Applications.* Nanomaterials (Basel), 2017. **7**(9).
41. William D. Callister, J., *Materials Science and Engineering. An Introduction*. Book. 2007.
42. Figueroa, A.I., *Magnetic nanoparticles. A Study by Synchrotron Radiation and RF Transverse Susceptibility.* Springer, 2014.
43. B.D.Cullity and C.D.Graham, *Introduction to Magnetic Materials, 2nd ed,.* (IEEE/Wiley, Hoboken, NJ, 2009).
44. Palihawadana-Arachchige, M., et al., *Gd-Doped Superparamagnetic Magnetite Nanoparticles for Potential Cancer Theranostics*, in *Nanostructured Materials - Fabrication to Applications*. 2017.
45. *Effect of Chemical Crosslinking on Properties of Polymer Microbeads: A Review.* Canadian Chemical Transactions, 2016: p. 473-485.
46. Ajay Vidyasagar, Jaroslaw Majewski, and R. Toomey, *Temperature Induced Volume-Phase Transitions in Surface-Tethered Poly(N-isopropylacrylamide) Networks.* Macromolecules, 2008(41): p. 919-924.
47. Yashin, V.V. and A.C. Balazs, *Theoretical and computational modeling of self-oscillating polymer gels.* J Chem Phys, 2007. **126**(12): p. 124707.
48. Yashin, V.V., O. Kuksenok, and A.C. Balazs, *Modeling autonomously oscillating chemo-responsive gels.* Progress in Polymer Science, 2010. **35**(1-2): p. 155-173.
49. Yoshida, R., *Self-oscillating gels driven by the Belousov-Zhabotinsky reaction as novel smart materials.* Adv Mater, 2010. **22**(31): p. 3463-83.
50. Chen, I.C., et al., *Shape- and size-dependent patterns in self-oscillating polymer gels.* Soft Matter, 2011. **7**(7).
51. Kuksenok, O., et al., *Exploiting gradients in cross-link density to control the bending and self-propelled motion of active gels.* Journal of Materials Chemistry, 2011. **21**(23).
52. Ryo Yoshida, et al., *In-Phase Synchronization of Chemical and Mechanical Oscillations in Self-Oscillating Gels.* Journal of Physical Chemistry A, 2000(104): p. 7549-7555.
53. Yuan, P., et al., *UV patternable thin film chemistry for shape and functionally versatile self-oscillating gels.* Soft Matter, 2013. **9**(4): p. 1231-1243.
54. Hill, T.L., *An Introduction to Statistical Thermodynamics*. 1960, Reading, MA: Addison-Weley.
55. Atkin, R.J. and N. Fox, *An Introduction to the Theory of Elasticity*. 1980, New York: Longman.
56. Onuki, A., *Theory of Phase-Transition in Polymer Gels.* Advances in Polymer Science, 1993. **109**: p. 63-121.

57. Chikazumi, S.O. and C.D. Graham, *Physics of Ferromagnetism.* (Oxford University Press, Oxford; New York), 2009. **2nd ed.**
58. Thirion, C., W. Wernsdorfer, and D. Mailly, *Switching of magnetization by nonlinear resonance studied in single nanoparticles.* Nat Mater, 2003. **2**(8): p. 524-7.
59. Petryayeva, E. and U.J. Krull, *Localized surface plasmon resonance: nanostructures, bioassays and biosensing--a review.* Anal Chim Acta, 2011. **706**(1): p. 8-24.
60. Griffiths, D.J., *Introduction to Electrodynamics.* 2013(Fourth eddition).
61. Luiza de Castro Folgueras*, M.A.A., Mirabel Cerqueira Rezende, *Dielectric Properties of Microwave Absorbing Sheets Produced with Silicone and Polyaniline.* Materials Research, 2010: p. 197-201.
62. Kuksenok, O., V.V. Yashin, and A.C. Balazs, *Three-dimensional model for chemoresponsive polymer gels undergoing the Belousov-Zhabotinsky reaction.* Physical Review E, 2008. **78**(4): p. 041406.1-041406.16.
63. Su, W.J., et al., *Dielectric relaxations of poly(N-isopropylacrylamide) microgels near the volume phase transition temperature: impact of cross-linking density distribution on the volume phase transition.* Soft Matter, 2014. **10**(43): p. 8711-8723.
64. Hirose, H. and M. Shibayama, *Kinetics of volume phase transition in poly(N-isopropylacrylamide-co-acrylic acid) gels.* Macromolecules, 1998. **31**(16): p. 5336-5342.
65. He, X.M., et al., *Synthetic homeostatic materials with chemo-mechano-chemical self-regulation.* Nature, 2012. **487**(7406): p. 214-218.
66. Wu, T., T.S. Rappaport, and C.M. Collins, *The Human Body and Millimeter-Wave Wireless Communication Systems: Interactions and Implications.* IEEE International Conference on Communications (ICC), 2015.
67. Kim, D., et al., *Programmable Volume Phase Transition of Hydrogels Achieved by Large Thermal Hysteresis for Static-Motion Bilayer Actuators.* Chemistry of Materials, 2016. **28**(23): p. 8807-8814.
68. Nemala, H., et al., *Investigation of magnetic properties of Fe3O4 nanoparticles using temperature dependent magnetic hyperthermia in ferrofluids.* Journal of Applied Physics, 2014. **116**(3): p. 034309.
69. Lang, C., D. Schuler, and D. Faivre, *Synthesis of magnetite nanoparticles for bio- and nanotechnology: genetic engineering and biomimetics of bacterial magnetosomes.* Macromol Biosci, 2007. **7**(2): p. 144-51.
70. Guimaraes, A.P., *Nanoscience and technology. Principles of nanomagnetism.* Springer Heidelberg Dordrecht London New York, 2009.
71. Jassal, M., A.K. Agrawal, and N.S. Save, *Thermoresponsive Smart Textile.* Indian Journal of Fibre Textile research, 2006. **31**: p. 52-65.